Design and Testing of an Electron Cyclotron Resonance Heating Ion Source for use in High Field Compact Superconducting Cyclotrons

by

Mark E. Artz

B.S., Civil and Environmental Engineering – 2010

Massachusetts Institute of Technology

SUBMITTED TO THE DEPARTMENT OF NUCLEAR SCIENCE
AND ENGINEERING
IN PARTIAL FULFILLMENT OF THE REQUIREMNTS FOR THE DEGREE OF

MASTER OF SCIENCE IN NUCLEAR SCIENCE AND ENGINEERING
AT THE
MASSACHUSETTS INSTITUTE OF TECHNOLOGY

SEPTEMBER 2012

Signature of Author: _____

Mark E. Artz
Department of Nuclear Science and Engineering
08-15-2012

Certified by: _____

Joseph V. Minervini
Division Head and Senior Research Engineer
Thesis Supervisor

Certified by: _____

Dennis G. Whyte
Professor
Thesis Reader

Accepted by: _____

Mujid S. Kazimi
TEPCO Professor of Nuclear Engineering
Chair, Department Committee on Graduate Students

Design and Testing of an Electron Cyclotron Resonance Heating Ion Source for use in High Field Compact Superconducting Cyclotrons

by

Mark Edward Artz

Submitted to the Department or Nuclear Science and Engineering
on August 15, 2012, in partial fulfillment of the requirements for the degree of
Master of Science in Nuclear Science and Engineering

Abstract

The main goal of this project is to evaluate the feasibility of axial injection of a high brightness beam from an Electron Cyclotron Resonance ion source into a high magnetic field cyclotron. Axial injection from an ion source with high brightness is important to reduce particle losses in the first several turns of acceleration within the cyclotron. Beam brightness is a measure of the beam current and rate of spread of the beam. The ultimate goal in developing an ECR ion source is to enable reduced beam losses along the entire acceleration path from the ion source through the cyclotron, allowing for a high beam current accelerator. Cyclotrons with high beam current have the potential to improve the availability of proton radiation therapy. Proton radiation therapy is a precisely targeted treatment capable of providing an excellent non-invasive treatment option for tumors located deep within tissue.

In order to model injection into high field it is necessary to measure the parameters of the beam extracted from the ion source. The two most important beam parameters are emittance and beam current. The emittance of the beam is a measurement of the rate of beam spread along the path of the beam and beam current is a measurement of the energy and quantity of particles within a charged particle beam.

This thesis presents the design and analysis of an ECR Ion Source and the instruments used to measure the emittance and beam current. Based on the modeling of the ECR ion source beam and the data gathered during testing, the ECR ion source presented in this thesis has the potential to provide a high brightness beam capable of high field axial injection. Beam simulations provide insight into the performance of the ECR ion source in high magnetic field. Axial beam injection from an external ion source is promising with moderate refinements to the ECR ion source.

Thesis Supervisor: Joseph Minervini
Title: Division Head and Senior Research Engineer

Table of Contents

Figure Index

Equation Index

1. Background

One of the most common uses of cyclotron particle accelerators is in proton radiation treatment. Proton radiation therapy is most advantageous in the treatment of tumors located deep within tissue because of the radiation dose can be precisely targeted avoiding surrounding organs. Radiation treatments with low tolerance for dose to surrounding tissue are the highest priority for receiving proton therapy. These cases commonly include children because proton therapy provides a reduced risk of secondary cancers. In adults, prostate, brain and spinal tumors are prime targets for proton therapy because of their close proximity to other sensitive organs such as the bladder and spinal cord.

Although proton therapy may have a fundamental advantage over other forms of radiation treatment it suffers from high costs and limited availability. In the United States there are only ten proton therapy facilities in operation, with each facility having construction costs well over $200 million dollars.

1.1. Proton Radiation Therapy Dose Distribution

The Bragg peak provides the basis for the fundamental advantage of proton therapy compared to other forms of radiation treatment. As a result of multiple Coulomb scattering, the amount of radiation dose deposited by a proton increases rapidly with depth. The loss of energy by a proton corresponds with peak dose before asymptotically decaying, Figure 1.1. Asymptotic decay of the proton depth dose curve allows for precise targeting of tumors located deep within healthy tissue. Figure 1.2 displays the radiation depth-dose curves for both protons and photons as they travel through water.

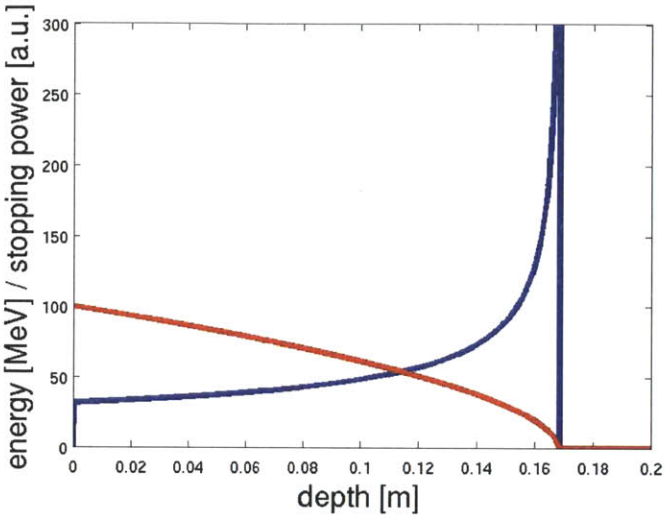

Figure 1.1 – 100 MeV Protons in Water - Asymptotic increase in stopping power shown in blue compared with the energy loss of the proton in red

The shape of the Bragg curve for protons is fundamentally different from the stopping power curve for x-ray, or photon, based radiation therapy. Unlike protons, photons deposit most of their energy as they enter a patient. The difference in shape of the depth dose curves of photons and protons is apparent in Figure 1.2. A majority of the radiation dose from photons is deposited near the surface, while for protons the dose is deposited much deeper. Figure 1.3 visualizes the distinct advantage provided by proton therapy through reduced dose to surrounding vital organs such as the heart.

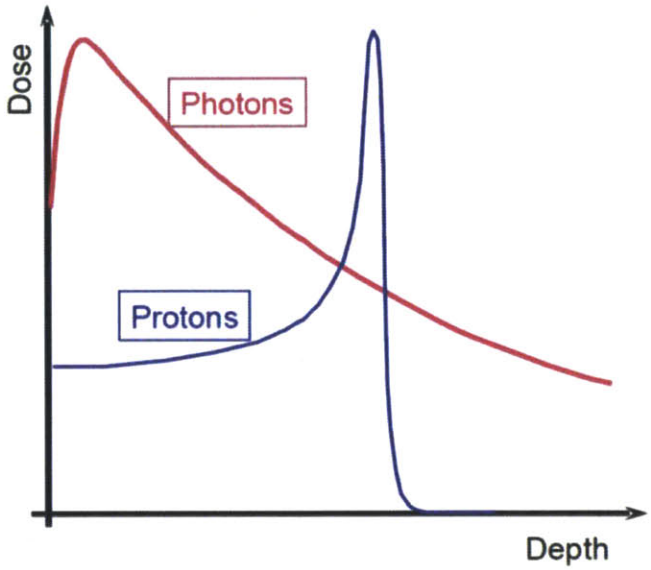

Figure 1.2 – Comparison of Depth-Dose curve for photons and protons

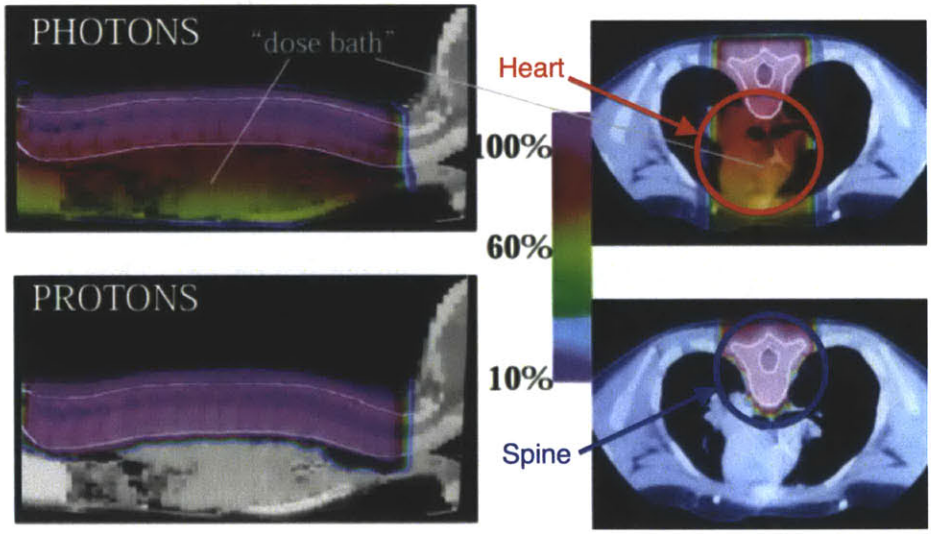

Figure 1.3 – Spinal dose bath of photons compared to proton therapy. Notice the reduced radiation dose to the heart achieved with protons

1.2. Cyclotron Particle Accelerators for Proton Therapy

Currently, isochronous cyclotrons are the primary type of particle accelerator used in proton therapy. Although isochronous cyclotrons are often large and expensive, they can provide a proton beam suitable for treating deep tissue tumors. The proton beam must achieve 230 MeV to be able to treat at depths of up to 35cm and provide several milliamps of beam current to supply a full radiation treatment dose to the tumor within a treatment interval lasting only a few minutes.

1.2.1. Isochronous Cyclotrons

Isochronous cyclotrons maintain a constant oscillation frequency of the accelerating electric field through all rotations of accelerating particles **[2]**. The magnetic field of an isochronous cyclotron must be designed to match the phase of the accelerating particles at each energy within the cyclotron. In order to maintain the same cyclotron frequency as the proton is accelerated, the magnetic field of the cyclotron must increase radially to match the relativistic mass increase. A radially increasing magnetic field is problematic because it defocuses the particles rotating within the cyclotron.

To combat the defocusing effect of the radially increasing magnetic field, the field gradient within the cyclotron can be reduced by decreasing the strength of the magnetic field and increasing the cyclotron's radius. This trade-off between field strength and beam defocusing has resulted in extremely large

cyclotrons shown in Figures 1.4 and 1.5. The relationship between magnetic field strength and cyclotron radius is shown in Figure 1.8.

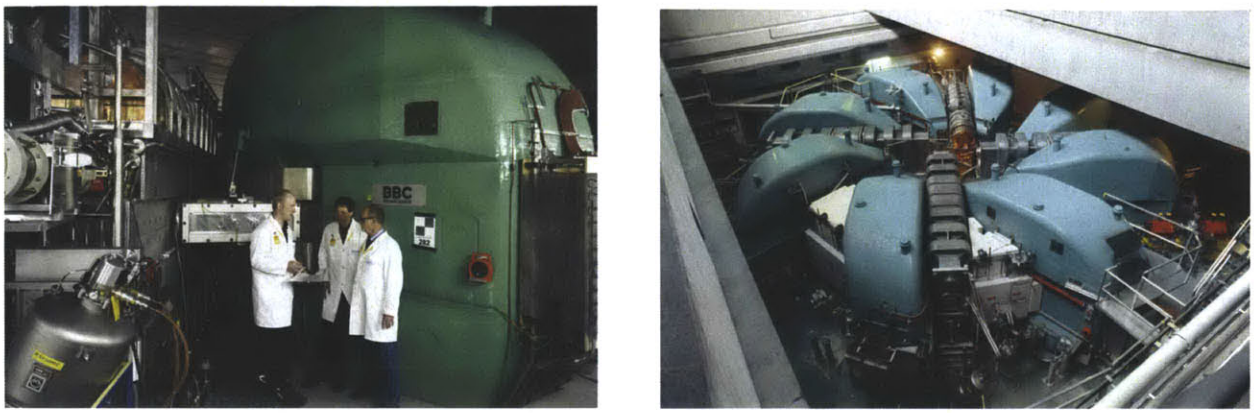

Figure 1.4 – 5.6 meter tall isochronous cyclotron located at the Paul Scherrer Institute

Figure 1.5 – 220 ton isochronous cyclotron being delivered to a new proton therapy facility in Seattle WA

1.2.2. Synchrocyclotrons

Synchrocyclotrons are attractive for compact cyclotron applications because they utilize a radially decreasing magnetic field, constantly focusing the particles accelerated within the cyclotron. The field profile of a synchrocyclotron requires that the frequency of oscillation of the accelerating electric field be varied to match the rotational frequency of the particles. This only allows one particle packet to be accelerated within the cyclotron at a time, significantly reducing the available beam current.

Since there can only be one particle packet accelerating in a synchrocyclotron at a time the beam current available from synchrocyclotrons is only on the order of nanoamps, where isochronous cyclotrons can provide milliamps. Reduced beam current increases patient treatment times and limits treatment options. This drastic variation in beam current becomes very important in radiation treatment planning because there is only a five-minute window to position and treat a patient before the process must be restarted.

1.2.3. Accelerator Constrained Treatment Options

Dose fractionation is the spacing of radiation treatments across several separate sessions. Fractionation utilizes the principle that healthy non-cancerous tissue is able to recover more quickly after radiation damage than cancerous tissue. This allows healthy tissue to recover more fully between radiation dose fractions than cancerous tissue. Radiation dose fractionation is

utilized in hopes that healthy tissue will survive and cancerous tissue will eventually die off.

The precise dose distribution available from proton therapy allows for promising treatment options using hypofractionated radiotherapy. Hypofractionation is the process by which fewer treatment sessions are used but with the same total delivered radiation dose. Hypofractionation with proton therapy is possible because proton therapy allows for more radiation dose to be targeted at the tumor, leaving the health tissue with less radiation damage. Figure 1.6, illustrates the cell survival of tumor and health tissue during normally fractionated radiation treatments. Figure 1.7 demonstrates how a hypofractionated treatment plan could allow for shorter treatment duration with an increased survival of health tissue.

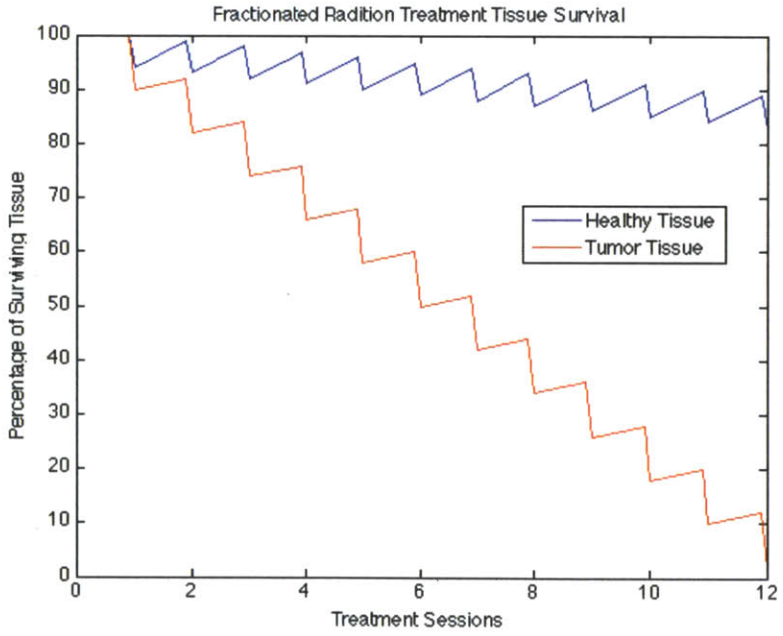

Figure 1.6 – Tissue survival during treatment with ordinary radiation dose fractions

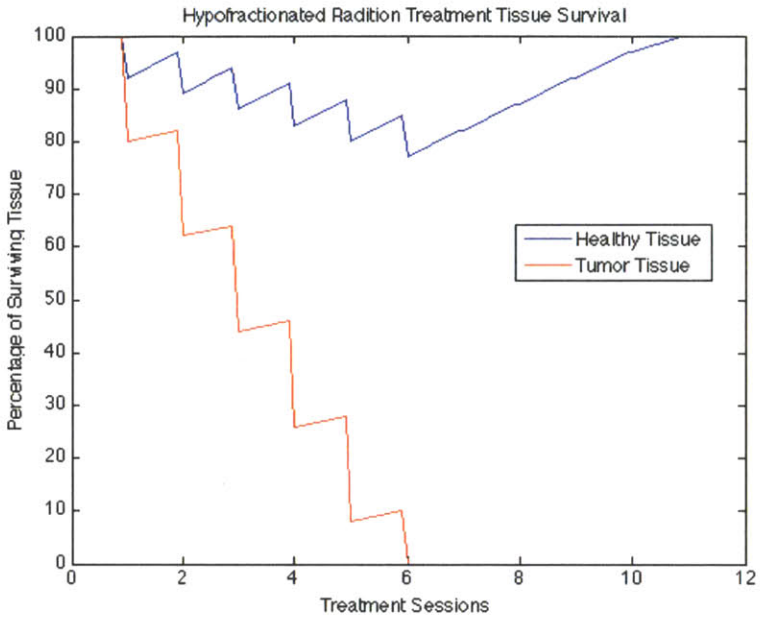

Figure 1.7 – Tissue survival during hypofractionated proton radiation treatment

1.3. High Field Isochronous Cyclotron for Proton Therapy

The ideal particle accelerator for proton therapy would be compact with high beam current. This would allow for promising treatment options such as hypofractionation as well as reducing the size and cost of facilities. Overall this could increase the availability of proton therapy throughout the United States and the world.

Synchrocyclotrons are attractive because they take advantage of the focusing

properties of a radially decreasing magnetic field. This allows synchrocyclotron to operate at high magnetic fields, significantly reducing their size. The relationship between field strength and cyclotron size is shown in Figure 1.8. Unfortunately, the limited beam current available from a synchrocyclotron create longer than desired treatment times and limit the possibility to further take advantage of the Bragg peak with hypofractionated treatment plans.

Magnetic Field Strength	Proton Extraction Radius	Fractional Size Reduction
B [T]	R [m]	$[R_1/R]^3$
1	2.28	1
3	0.76	1/27
5	0.46	1/125
7	0.33	1/343
9	0.25	1/729

Figure 1.8 – Radial size reduction with increasing cyclotron magnetic field [2]

Ultimately, the most attractive option for an accelerator for use in proton therapy would be a high field isochronous cyclotron that makes use of a proton ion source that provides a pre-focused beam. Injection of a prefocused proton beam could alleviate come of the size restrictions created by the defocusing effects of a radially increasing magnetic field within and isochronous cyclotron. This could be accomplished with an Electron Cyclotron Resonance, ECR, heating ion source

axially injected into a high field cyclotron. This thesis describes the design and testing of an ion source capable of providing a proton beam attractive for axial injection into a cyclotron. In order for the ECR ion source to be attractive for axial cyclotron injection, the ion source should provide a 20mA proton beam with 20keV particle energy maintained within a 1cm radius for a linear path of 76cm. The length of 76cm is significant because it represents the distance to the accelerating plane of the compact high field cyclotron used in beam simulations.

2. Physics of an Electron Cyclotron Resonance Ion Source

This section will describe the underlying physics used in the design of an Electron Cyclotron Resonance ion source including ion production, extraction and beam characteristics. Matching the electron cyclotron frequency in a static magnetic field with the frequency of the microwave-heating source ionizes hydrogen gas within an ECR ion source. These ions are extracted across a high electric potential, accelerating them away from the ion source. The quality of the extracted particle beam can be described in terms of emittance, brightness and beam current.

2.1. Main Ion Source Components

The following section will identify the main components that form an ECR ion source. These components are essential to the ionization of hydrogen and extraction of a charged particle beam.

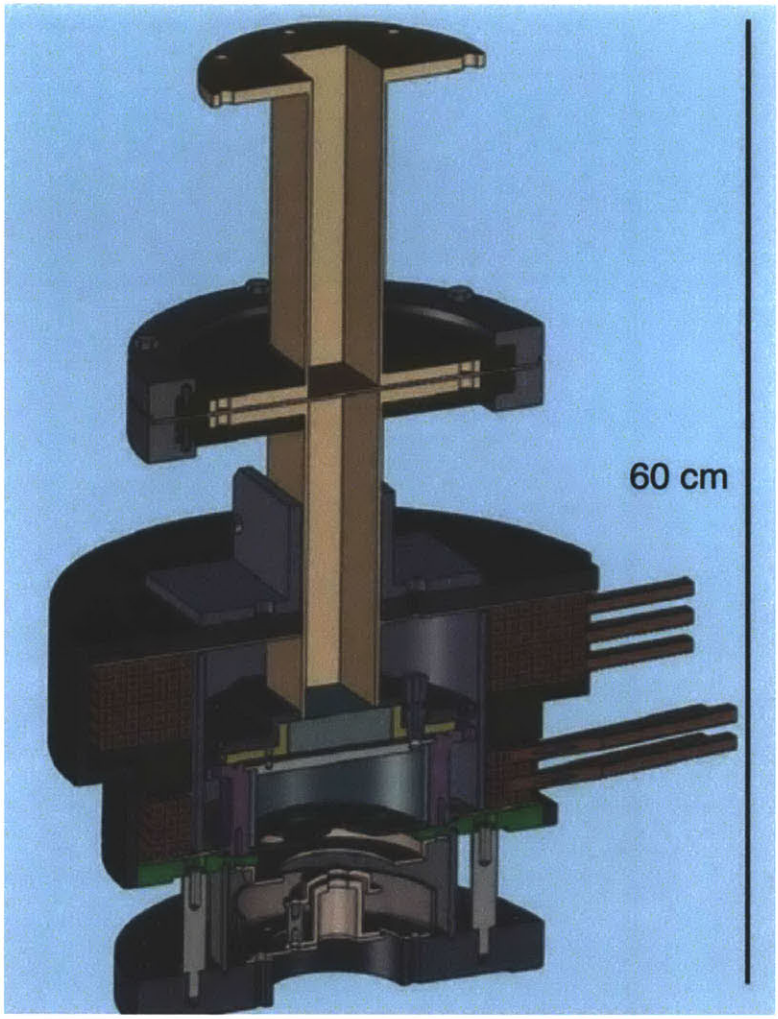

Figure 2.1 – A cross section of the axysymmetric cyclyndrical ECR ion source. The total height of the ion source assembly is 60 cm

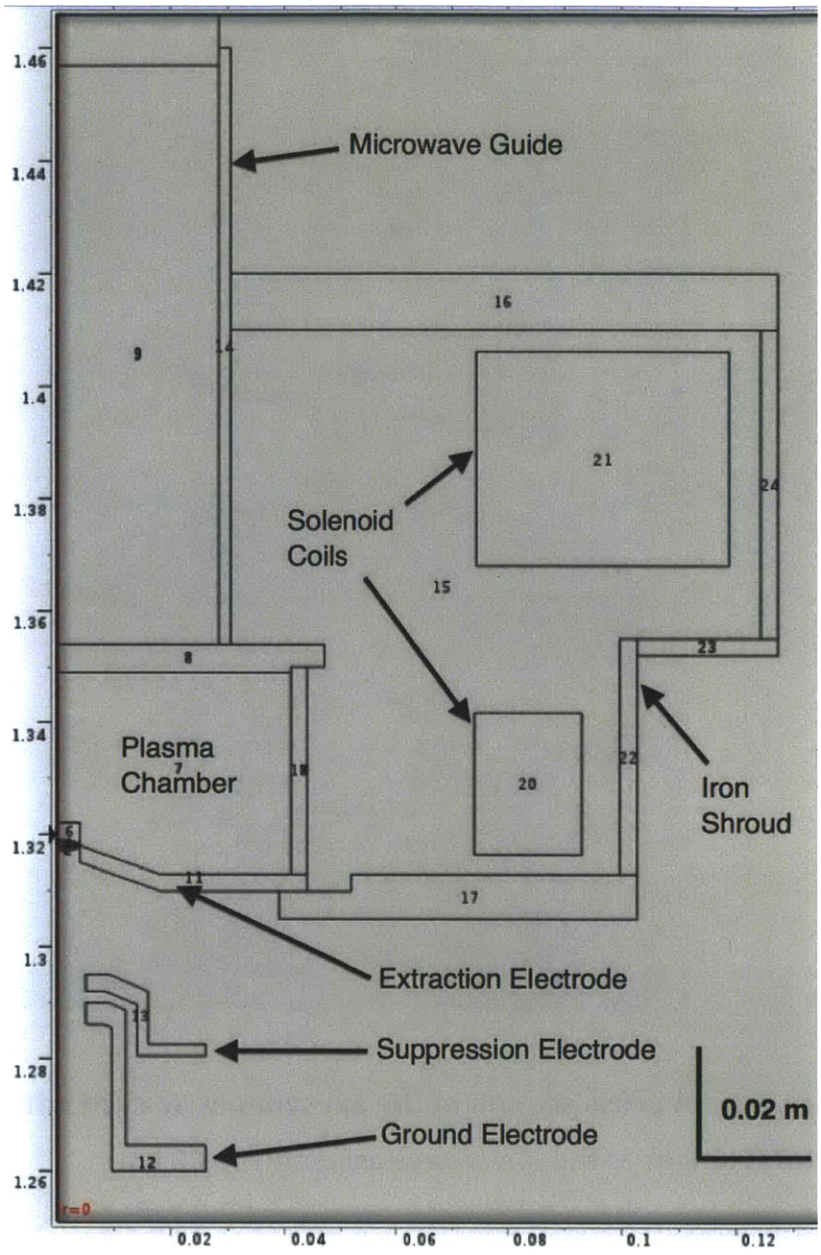

Figure 2.2 – Axissymmetric cylindrical cross section of the ion source. The verical and radial scale are given in meters. The height is given in meters above the floor of the laboratory where the ion source was designed to be tested

2.1.1. Electrodes

The electrodes of the ion source are used to create a large electric potential gradient to allow extraction and acceleration of positively charged ions. The electrodes of the ion source are components 11, 12 and 13 in Figure 2.2. Figure 2.3 shows the electric potential along the axis of the ion source. The maximum and minimum electric potential along axis correspond to the locations of the ion source electrodes.

The extraction electrode is component 11 in Figure 2.2. It is held at a constant high postive electric potential relative to the ground electrode. This potential can be varied depending upon the operation of the ion source from 5,000 to 20,000 volts.

The suppression electrode is component 13 in Figure 2.2, it is held at a constant electric potential of -2,000 volts relative to the ground electrode. The negative potential of the susspression electrode creates an electric potential barrier, preventing free electrons from back-streaming into the ion source.

The ground electrode, component 12, completes the electric potential.

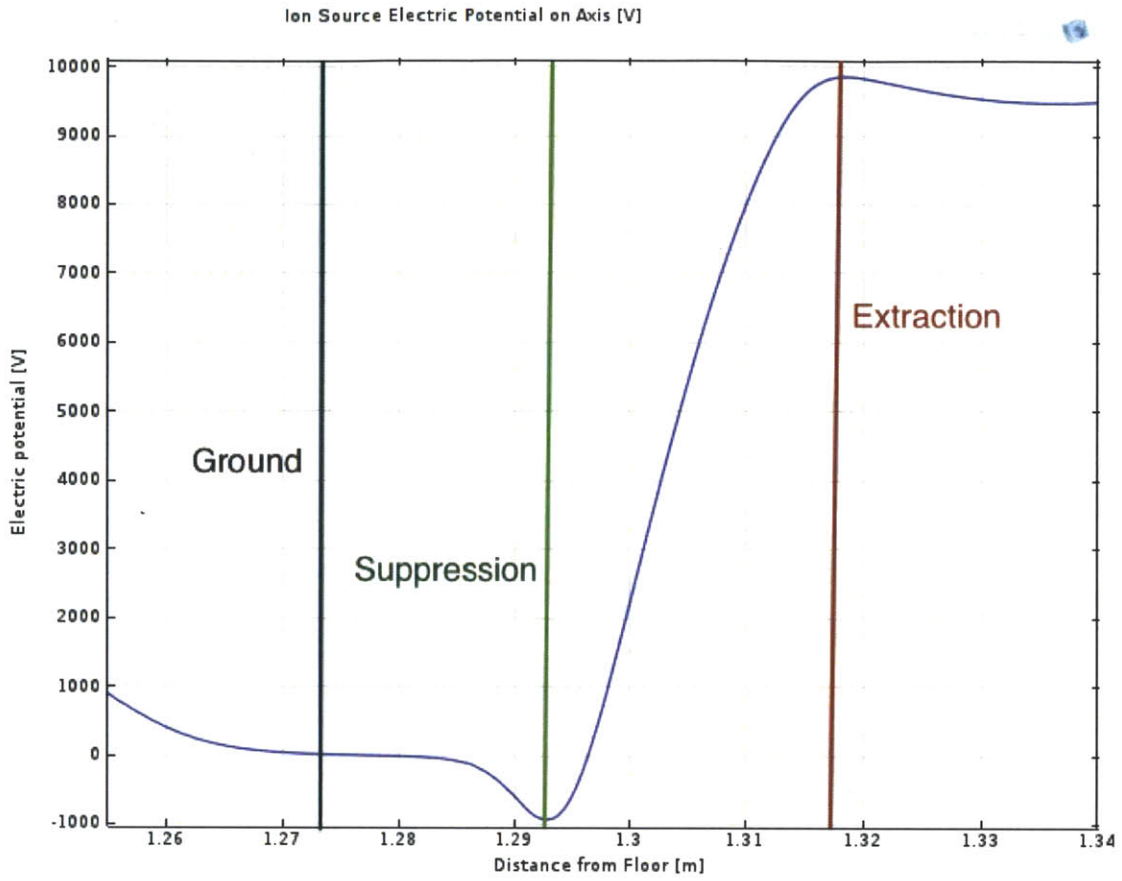

Figure 2.3 – The electric potential along the center axis of the ion source. The minimum electric potential correspondes to the location of the supression electrode. The maximum electric potential corresponds to the location of the extraction electrode. The horizontal scale corresponds to the vertical location of the components shown in Figure 2.2, both in meters

2.1.2. Solenoid Coils for Resonant Magnetic Field

Components 20 and 21 in Figure 2.2, are solenoid coils with current density tuned to provided a magnetic field of 0.0875 Tesla within the plasma chamber. A magnetic field of 0.0875 Tesla results in an electron cyclotron frequency of 2.45GHz. The design of the solenoid coils is discussed in more detail in section 3.

2.1.3. Iron Shroud

The iron shroud is formed by components 16, 17, 22, 23, and 24. It is kept at the same high voltage as the extraction electrode and influences the shape of the magnetic field generated by the solenoid coils.

2.1.4. Microwave Guide

The microwave guide, component 9 in Figure 2.2, is located directly above the plasma chamber and provides a path for 2.45 GHz microwaves to energize free electrons and ionize hydrogen gas located in the plasma chamber. The processes of electron cyclotron heating is described in more detail in section 2.2.

2.1.5. Plasma Chamber

The plasma chamber, component 7 in Figure 2.2, is the location of the ionization of hydrogen gas to form a plasma, consisting of both hydrogen ions and electrons. The plasma housed in this section of the ion source provides the positive hydrogen ions that compose the extracted beam.

2.2. Electron Cyclotron Resonance Heating

The electron cyclotron resonance frequency is determined by equating the Lorentz Force, equation 2.1, to the centripetal force, equation 2.2.

$$F = q(E + v \times B) \qquad \textbf{eq. 2.1}$$

$$F = m_e \omega^2 r \qquad \textbf{eq. 2.2}$$

$$q = 1.602 \times 10^{-19}\ [Coulombs]$$
$$m_e = mass\ of\ electron = 9 \times 10^{-31}\ [kg]$$
$$B = magnetic\ field\ [Tesla]$$
$$E = electric\ field\ [Volts/meter]$$

The only component of the particle velocity that is transverse to the direction of the magnetic field is in the theta direction. Using this information one can solve for the electron cyclotron frequency, f_{ec}.

$$E = 0$$
$$v_\theta = \omega r$$
$$q\omega r B = m_e \omega^2 r$$
$$\omega = \frac{qB}{m_e} = \frac{1.6\times10^{-19}C}{9\times10^{-31}kg} B$$
$$f = \frac{\omega}{2\pi} = \frac{1.8\times10^{11}}{2\pi}$$
$$f_{ec} = 28\times B\ GHz$$

The most commonly available microwave heating systems operate at 2.45 GHz. Using this value for the electron cyclotron frequency one can determine the value of the magnetic field required for resonance heating. The resonant magnetic field for electrons heated with 2.45 GHz microwaves is 0.0875 tesla.

2.3. Ion Production

An ECR ion source uses electron cyclotron resonance heating to ionize a gas and form a plasma of positive and negatively charged ions. The molecules of the gas are ionized by collision with high energy free electrons created by electron cyclotron heating. These high energy free electrons must be accelerated above the ionization energy of the gas molecules to have sufficient energy to cause ionization. As the gas is ionized more free electrons are produced creating an avalanche effect ultimately resulting in the production of a plasma. The positive ions of the plasma can be extracted and accelerated across an electric potential gradient to form a particle beam.

The dominant electron reactions for the ionization of hydrogen gas in an ECR ion source are listed in equation 2.3. The most prevalent ion species extracted from ECR ion sources depends on the configuration and operating parameters of the ion source. For ion sources similar to the one described in this thesis the most common species is often H^+ **[25]**. This thesis will focus on positive hydrogen ions, because they are expected to compose a majority of the ion species extracted from the ion source.

$$H_2^+ + e \longrightarrow H^+ + H + e$$

$$H + e \longrightarrow H^+ + 2e$$
$$H_2 + e \longrightarrow H_2^+ + e$$

eq. 2.3

2.4. Beam Current

Beam current is a measure of the electric charge in Coulombs transported per second. The Child-Langmuir Law, equation 2.4, describes the maximum beam current in a space charge limited beam extracted from an ion source.

$$I_{max} = \frac{4\epsilon_0\left(\frac{2q}{m_p}\right)^{\frac{1}{2}} S\, V_{ex}^{\frac{3}{2}}}{9D^2}\ [C/s] \qquad \textbf{eq. 2.4}$$

$I_{max} = Maximum\ Beam\ Current\ [Coulombs/second]$
$\varepsilon_0 = permittivity\ of\ free\ space$
$= 8.85 \times 10^{-12}\ [F/m]$
$q = 1.602 \times 10^{-19}\ [Coulombs]$
$S = surface\ area\ of\ extraction\ electrode\ [m^2]$
$D = distance\ between\ electrodes\ [m]$
$V_{ex} = extraction\ voltage\ [Volts]$
$m_p = mass\ of\ proton\ [kg]$

For the electrode geometry described is this thesis, S = $\pi \times .01^2$ [m^2] and D = 0.03 [m], the Child-Langmuir Law results in a maximum beam current of 40 mA at an extraction voltage of 10 kV. A beam current of this magnitude is not likely to be achievable with a prototype ECR ion source design. For a preliminary test of the ion source it may be reasonable to expect 5% of the I_{max}, or about 2mA. The extracted beam current will most likely be limited by operating parameters such as extraction voltage, vacuum quality, gas flow rates and microwave heating power.

In order to simulate various beam current values below I_{max}, it is useful to calculate the number of particles extracted from the ion source. The rate of particle extraction can be calculated using equation 2.5.

$$N = \frac{I}{q} \left[\frac{particles}{s}\right] \qquad \textbf{eq. 2.5}$$

$N = particles\ per\ second$
$I = beam\ current\ [amperes]$
$q = 1.602 \times 10^{-19}\ [Coulombs]$

2.5. Beam Characteristics

In addition to beam current, emittance and beam brightness are also important characteristics when describing a charged particle beam. Emittance describes the rate of spread of a beam of charged particles. Beam brightness provides information about both beam current and emittance. Very bright beams have both large beam current and low emittance.

2.5.1. Emittance

Emittance is plotted in phase-space with the radial location of the particles plotted against the ratio of radial and longitudinal velocity, $x' = v_r/v_z$. The direction of the beam path is designated as the z-direction and the radial distance from the center of the beam is designated as the r-direction, $x = r$.

The emittance ellipse is given as a statistical feature of the beam based on the percentage of the beam it encompasses. The measure of emittance is calculated from the Root Mean Squared error, RMS, of the phase space plot. The RMS for a charged particle beam is measured in units of length times an angle, $m \cdot rad$. Emittance is usually reported in $mm \cdot mrad$ for convenience.

Equation 2.6 shows the calculation of one unit of RMS. The area of an emittance ellipse with one RMS unit generally encompasses about 68% of the beam data. It is common to enlarge the emittance ellipse to encompass 95% of the beam data. For most Gaussian shaped beams, 95% of the beam data is enclosed in an emittance ellipse corresponding to $4 \cdot \text{RMS}$. Within this thesis, emittance ellipses are calculated to encompass 95% of the simulated beam data and the RMS emittance is reported in $mm \cdot mrad$.

The Twiss parameters, α, β, and γ, govern the size and shape of the emittance ellipse and follow the relation in equation 2.7 **[25]**. The particle data displayed on the phase space plot is used to calculate the emittance, E_{rms}, and Twiss parameters shown below.

One of the most informative parameters of the emittance ellipse is its angle of rotation, theta. An emittance ellipse that is tilted to the right, like in Figure 2.4, shows a beam that is diverging, while an emittance ellipse that is tilted to the left is converging.

$$E_{rms} = \sqrt{\langle x^2 \rangle \cdot \langle x'^2 \rangle - \langle x \cdot x' \rangle^2} \quad [m \cdot rad] \qquad \textbf{eq. 2.6}$$

$$\beta\gamma - \alpha^2 = 1 \qquad \textbf{eq. 2.7}$$

$$x = \ radial\ distance\ from\ beam\ center \quad [m]$$

$$x' = {}^{v_r}/_{v_z}$$

$$\alpha = {}^{\langle x \cdot x' \rangle}/_{E_{rms}} \quad [rad^{-1}]$$

$$\beta = {}^{\langle x^2 \rangle}/_{E_{rms}} \quad [m/rad]$$

$$\gamma = {}^{\langle x'^2 \rangle}/_{E_{rms}} \quad [(m \cdot rad)^{-1}]$$

$$\gamma \cdot x^2 + 2 \cdot \alpha \cdot x \cdot x' + \beta \cdot x'^2 = {}^{Area}/_{\pi} = E_{rms}$$

$$\frac{b}{a} = \frac{\alpha}{\beta} + {}^{(\beta+\gamma)}/_{2} + {}^{\left(\sqrt{(\beta+\gamma)^2 - 4}\right)}/_{2} \qquad \textbf{eq. 2.8}$$

$$\tan(2\theta) = \frac{2\alpha}{\gamma - \beta}$$

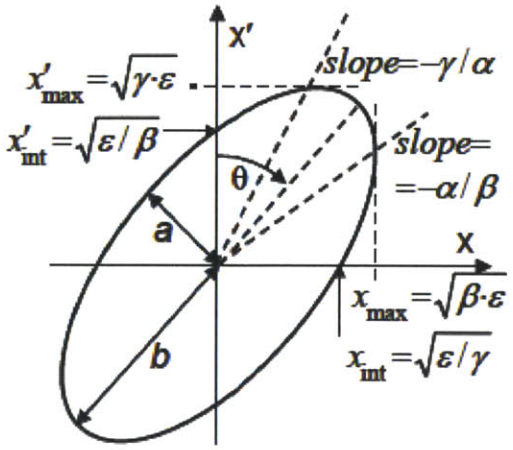

Figure 2.4 – Relation of the Twiss parameters to the shape of the emittance ellipse

2.5.2. Brightness

Brightness is a beam quality indicator that captures the beam current per unit of the product of emittance area in the beam's two transverse directions, i.e. x and y by our definitions, given in equation 2.9. Ideal beams for injection into cyclotrons would be very "bright", having large beam current and low emittance.

$$B\left[\frac{Amps}{(m \cdot rad)^2}\right] = \frac{I[Amps]}{\pi^2 \cdot E_x[m \cdot rad] \cdot E_y[m \cdot rad]} \qquad \textbf{eq. 2.9}$$

3. Coil Design for Electron Cyclotron Resonance Heating

This section describes the design of the solenoid coils that are used to produce the resonant magnetic field within the plasma chamber of the ion source. For 2.45 GHz microwaves a resonant magnetic field of 0.0875 Tesla is required to energize electrons and ionize hydrogen gas.

In order to achieve the 0.0875 Tesla magnetic field required for electron cyclotron resonance heating, two solenoid coils are used. The magnetic field produced by the ECR solenoid coils was simulated originally using Poisson Superfish **[7]** and later with COMSOL for use in beam extraction simulations. Figure 3.1 displays the locations of resonant magnetic field within the ion source.

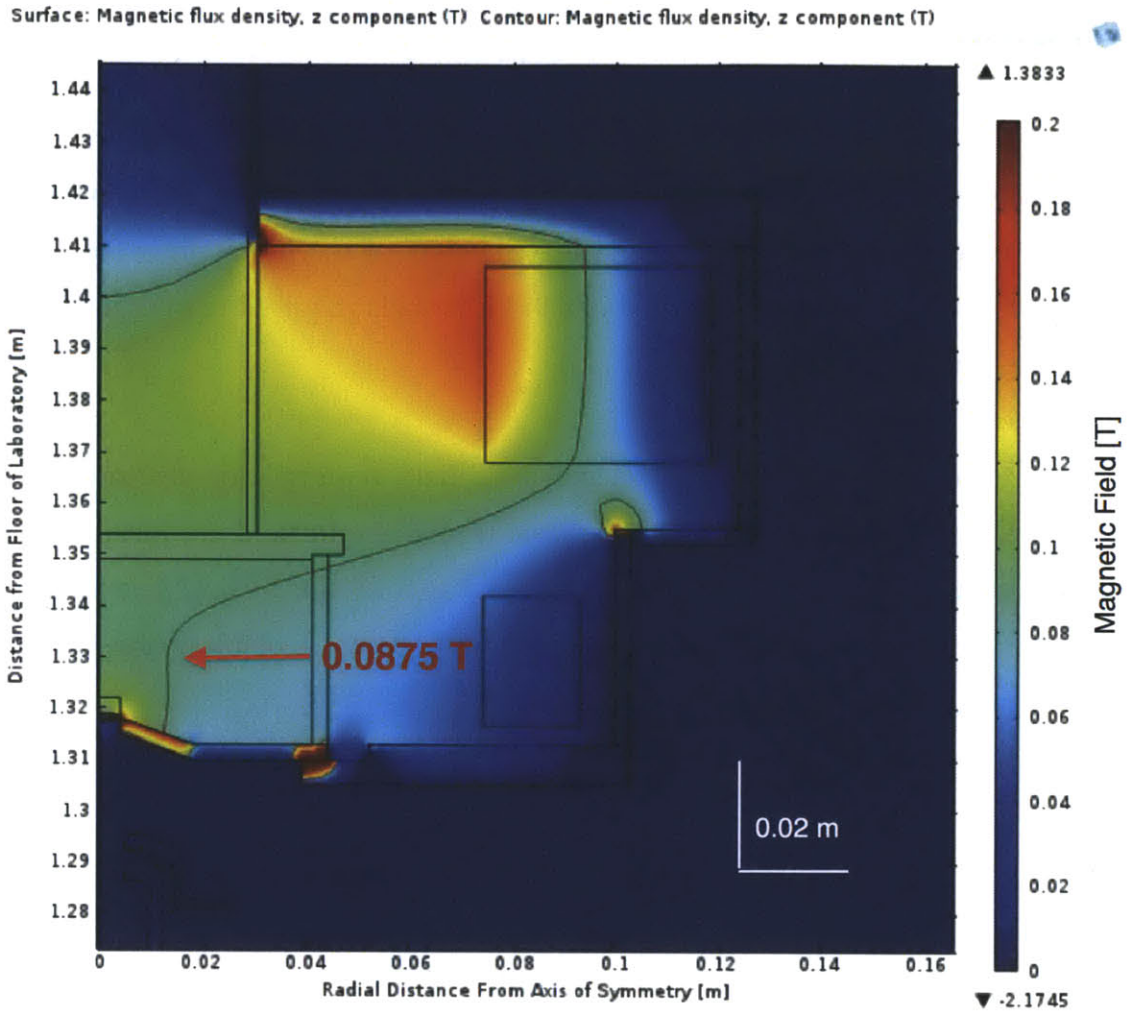

Figure 3.1 – Axisymmetric cylindrical cross section of the ECR ion source. The region of 0.0875T within the plasma chamber is shown with the red contour. The magnetic field provides for resonant electron ionization and heating at the electron cyclotron frequency of 2.45GHz

Figure 3.2 shows the magnetic field on axis within the ion source. The saddle shape helps to provide magnetic mirroring and improves plasma confinement.

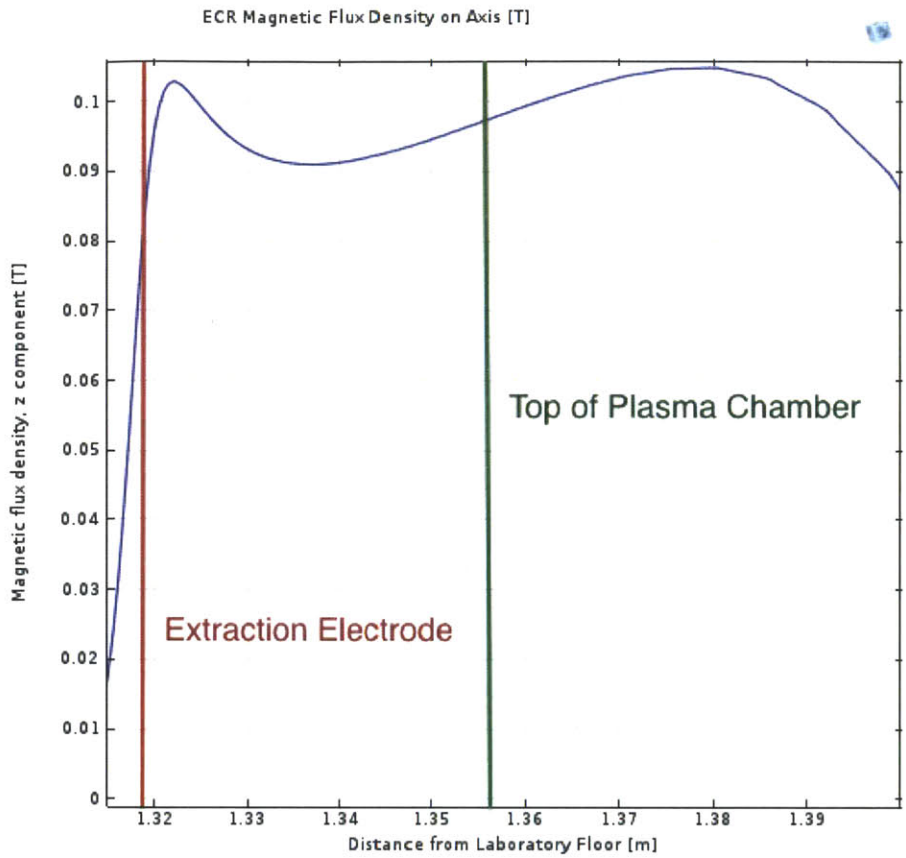

Figure 3.2 – Magnitude of ECR magnetic field along axis of symmetry. The ECR magnetic field falls off abruptly below 1.32 m due to an iron extraction electrode

3.1. ECR Solenoid Coil Design Considerations

When designing the solenoid coils for use in the ECR it was important to incorporate electrical insulation from high voltage components of the ion source. In

addition to electrical insulation, hollow copper conductor was selected large enough to provide adequate current capacity and water cooling.

3.1.1. Ease of Winding

The ECR solenoid coils were formed using an aluminum winding cylinder and cured with epoxy. In order to simplify the winding process both coils have the same inner radius as well as an even number of vertically stacked coils, allowing for the use of a double pancake winding technique. The double pancake winding technique requires an even number of stacked coils. First, the bottom pancake is wound and then the top of the double pancake. This winding technique results in two coils stacked on top of each other that terminate at the outer radius of the solenoid. **[12]**

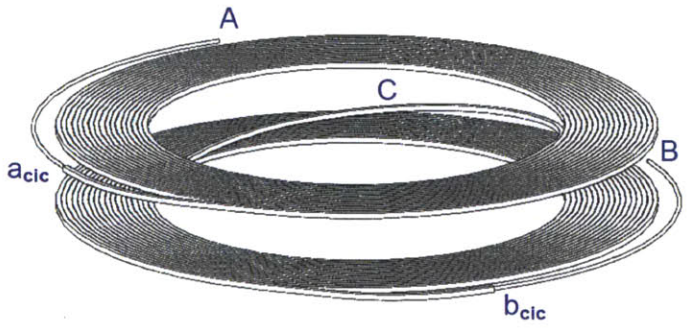

Figure 3.3 – A double pancake solenoid wind is begun in the center with both the upper and lower "pancake" being wound outwards

3.1.2. High Voltage Insulation

The ion source solenoid coils are floated at ground potential, located within the high voltage iron shroud. The close proximity of the ground potential solenoid coils to the high voltage iron shroud makes electrical insulation necessary to prevent arcing. The dielectric strength of air is only 3×10^6 V/m and the extraction voltage of the ion source is 10 kV, any part of the ion source floated at ground potential located within 14mm of high voltage must have a stronger dielectric to prevent arcing.

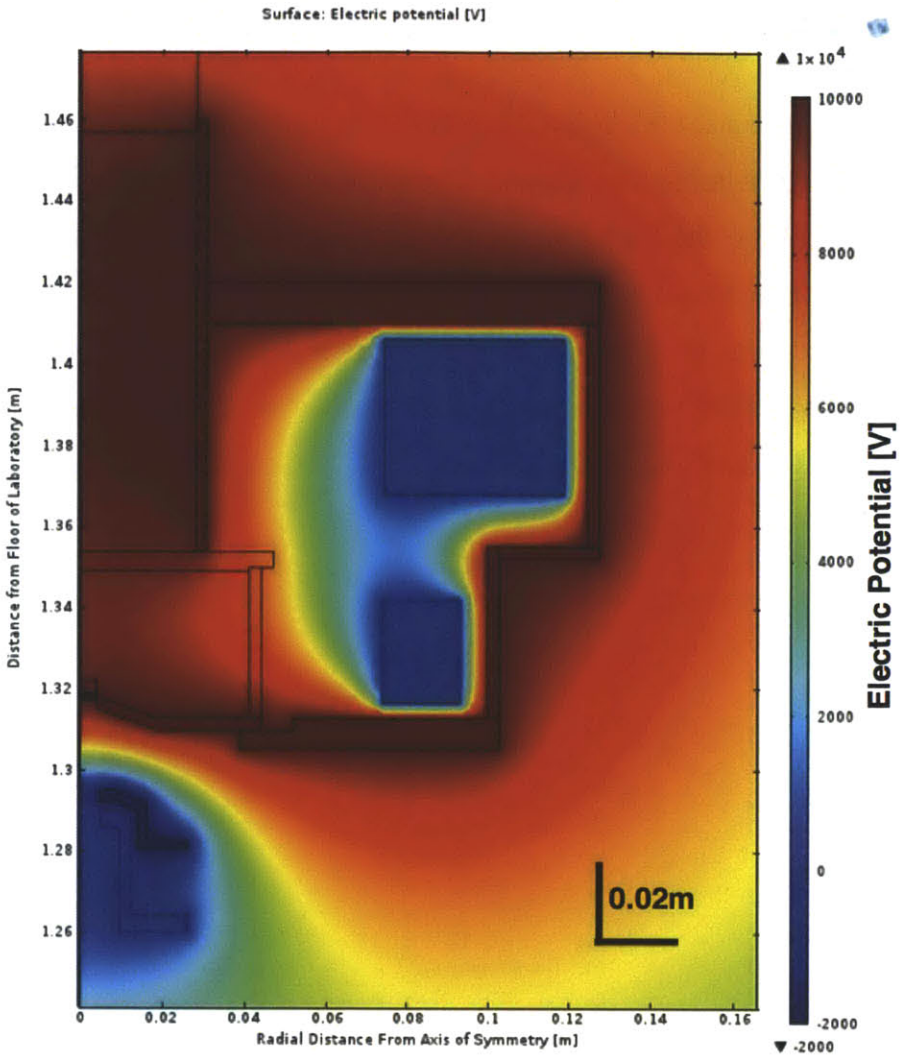

Figure 3.4 – Axisymmetric cylindrical cross section of the ECR ion source showing the electric potential of components within the ion source. Notice the strong gradient on the outer edge of the coils; arcing across this gradient ultimately limited the extraction voltage

To prevent arcing across the ion source components floating at ground, a Teflon ring was placed between the waveguide and the inner edge of the

solenoid coils, as labeled in Figure 3.5. Teflon has a dielectric strength of 20 kV/mm, about seven times stronger than air. The other edges in close proximity to high voltage were insulated with Kapton, which has a dielectric strength of about 100 kV/mm, about 30 times stronger than air.

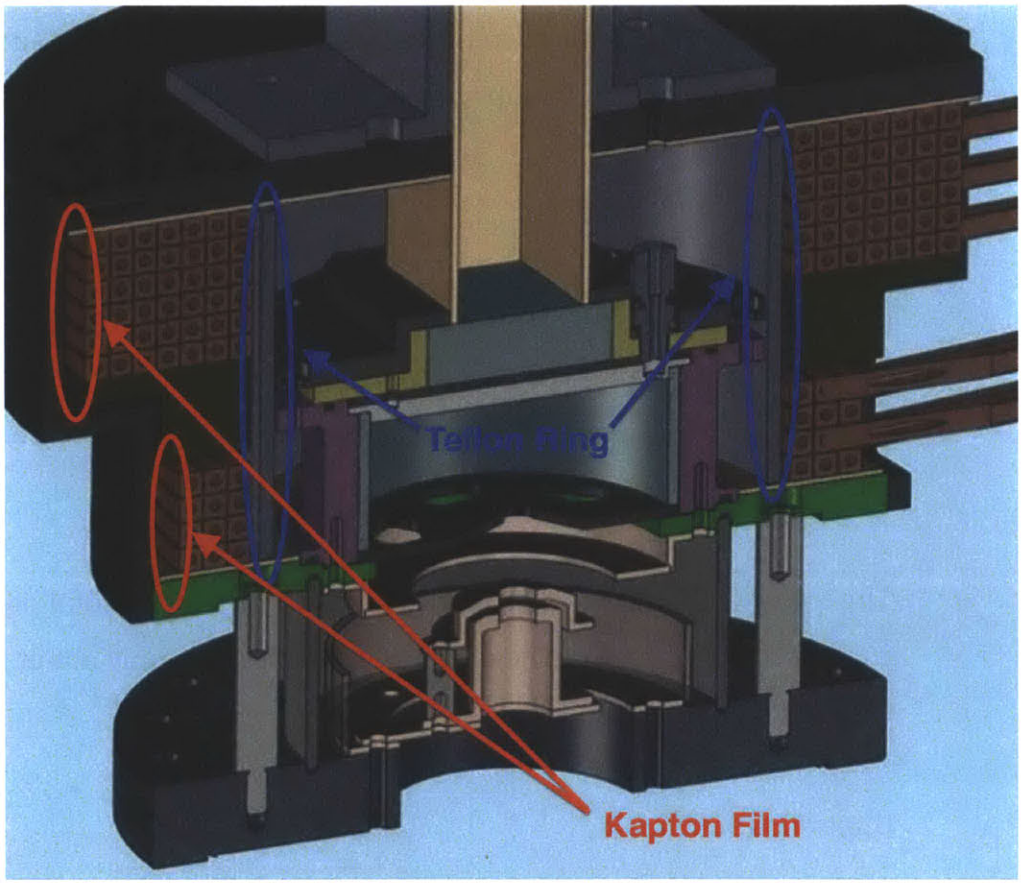

Figure 3.5 – ECR ion source cross section showing Teflon ring on the inside of the solenoid coils, circled in blue, and Kapton film on the outside surfaces of the coils, circled in red, provide protection against arcing

3.1.3. Resistive Heating

In order to achieve a field of 0.0875 T within the plasma chamber it is necessary to have high current density in the larger solenoid coil of the ion source. With nearly 170 amps of current flowing through the coil, over heating becomes a concern.

Based on the cross sectional area of the conductor used in the coils, the conductor has a resistance of 0.006 ohms/m. The upper coil also has an inner radius of 10cm with 6 layers each having 7 turns for a total of 48. This results in a total length of about 30 meters for the top coil and a total resistance of 0.18 ohms.

The lower coil only has 4 layers each with 3 turns for a total of 12 turns and a current of 43 amps. Total length of the lower coil is only about 8 meters and a total resistance of 0.48 ohms.

Upper Coil:

$$V = 170\ amps \times 30\ m \times 0.0006\ \frac{ohms}{m}$$
$$V = \sim 3\ volts$$

$$Power = I^2R$$
$$Power = 520\ Watts$$

Lower Coil:

$$V = 43\ amps \times 8\ m \times 0.0006\ \frac{ohms}{m}$$

$$V = \sim 0.2\ volts$$

$$Power = 9\ Watts$$

The voltage drop across the coils was verified with a voltage meter. During operation of the ion source the upper coil produces enough heat that it will require water cooling while the lower coil will not.

3.1.4. Water Cooling of Upper Solenoid Coil

Based on the calculation of the power dissipated by the coil it will be desirable to water cool the larger solenoid coil in the ion source. Using the water pressure from the faucet should be adequate but it is still a good idea to ensure there is sufficient water pressure to supply the full length of coil. By estimating the pressure drop across the length of the coil using the Bernoulli equation with viscous losses, one can determine if typical household water pressure of 550 kPa (80 psi) will be sufficient for the length of the larger ECR solenoid coil.

The Bernoulli equation states that the normalized pressure, head, along a streamline is constant.

$$h = z + \frac{P}{\rho g} + \frac{v^2}{2g}$$

$$z = height\ [m]$$
$$P = pressure\ [Pascal]$$
$$v = velocity\ \left[\frac{m}{s}\right]$$

The Bernoulli equation above does not take into account energy in real viscous fluids. To take energy loss into account the viscous head term must be introduced as shown in equation 3.2.

$$h = z + \frac{P}{\rho g} + \frac{v^2}{2g} + \int_{x_0}^{x} \frac{f}{D}\frac{v^2}{2g}\,dx \qquad \textbf{eq. 3.1}$$

$$f = friction\ factor$$
$$D = pipe\ diameter\ [m]$$

The friction factor, *f*, is used to scale the viscous head by the parameters of the pipe. It is a function of the Reynolds number, Re, a ratio of the inertia to the viscosity within the pipe.

$$f = \frac{64}{Re}$$
$$Re = \frac{\rho v D}{\mu}$$
$$\mu = viscosity\ [Pa \cdot s]$$

Using the viscous head term from equation 3.2 one can estimate the pressure drop across the larger ECR solenoid coil. The hollow copper conductor used to make the ECR coils has an inner diameter of 3mm. It is also common to limit the velocity of water in household systems below 2m/s to prevent pipe

vibration, for the purpose of this estimation a more conservative 1 m/s was used:

$$\Delta P = \int_{x_0}^{x} \frac{f}{D}\frac{v^2}{2g}\,dx$$

$$\Delta P = \rho g\left(f\frac{L}{D}\frac{v^2}{2g}\right)$$

$$Re = \frac{\rho v D}{\mu} = \frac{10^3\,\frac{kg}{m^3}\cdot 1\frac{m}{s}\cdot 0.003\,m}{10^{-3}Pa\cdot s} = 3\cdot 10^3$$

$$f = \frac{64}{Re} = \frac{64}{3\cdot 10^3} = 0.021$$

$$\Delta P = \rho g\left(f\frac{L}{D}\frac{v^2}{2g}\right) = 10^3\cdot 9.81\left(0.021\cdot\frac{30}{.003}\cdot\frac{1}{2\cdot 9.81}\right)$$

$$\Delta P = 105\,kPa$$

Based on this analysis, the pressure drop across the length of the upper ECR solenoid coil is less than the pressure available from a household faucet. A 550 kPa water line should be sufficient to provide adequate flow to the larger ion source solenoid coil.

4. Beam Simulation

This section describes the method used to simulate the charged particle beam extracted from the ion source as well as the post processing developed to evaluate the emittance of the beam at various locations along the beam path.

4.1. Charged Particle Tracing

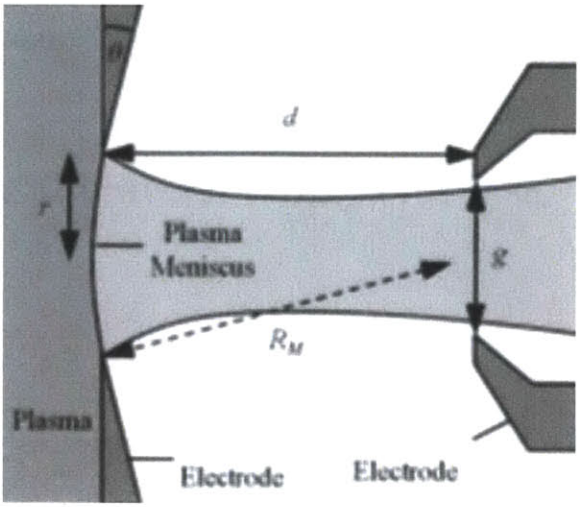

Figure 4.1 – The plasma meniscus is used as the particle emitting surface in beam simulations. The particles emitted on this surface were given a randomized velocity. For the case shown here the meniscus is concave

The plasma meniscus, as shown in Figure 4.1, is used as the surface for emitting charged particles for beam simulations within this thesis. The concavity of the

plasma meniscus is not known through the design of the ECR ion source but will be estimated by comparing the measured particle distribution with simulation.

Figure 4.2 shows the surfaces used to represent the plasma meniscus during beam simulations. These surfaces are elliptical approximations of the plasma meniscus with a major radius of 4mm and minor radii of 0mm (flat), 0.5mm, and 1mm, as compared to the major radius of 4mm, set by the extraction electrode aperture. Both concave and convex plasma meniscus shapes were simulated.

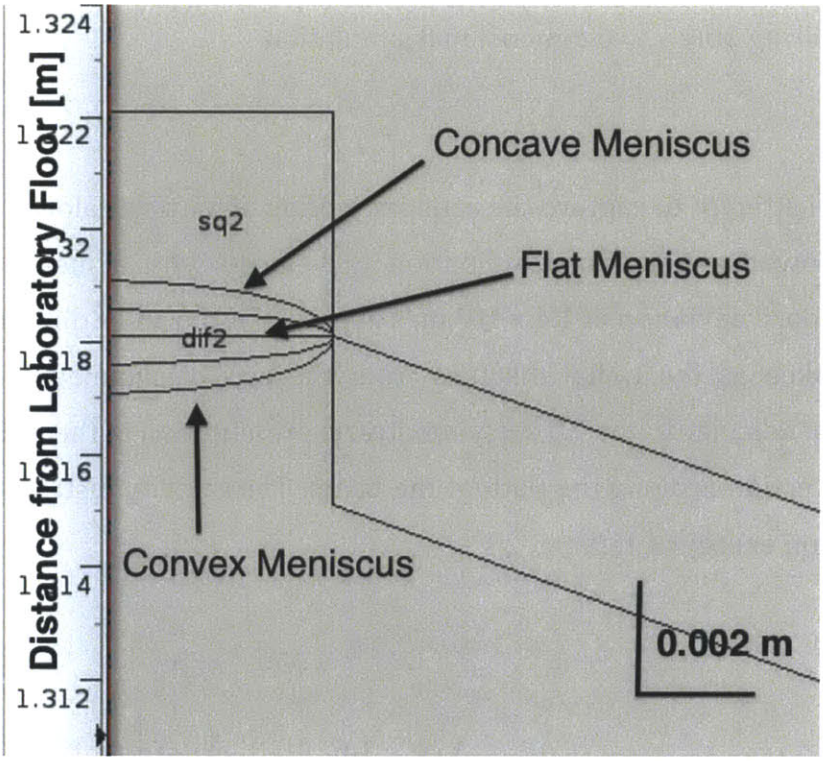

Figure 4.2 – Axisymmetric cylindrical cross section of extraction electrode aperture. Several particle emitting surfaces used to represent the plasma

meniscus are indicated. The scale on left is given is meters from the laboratory floor

In order to simulate the beam path from the extraction electrode on the ion source the charged particle tracing code available as part of the COMSOL simulation software was used. COMSOL allows for particles to be emitted from a surface with an initial velocity distribution in three dimensions. COMSOL solves for the particle trajectories using the Lorentz and electrostatic forces, taking into account both magnet and electric field. The ion source and beam path are axisymmetric, requiring only a two dimensional simulation.

In an attempt to capture the random motion of particles along the plasma meniscus I allowed a Gaussian distribution of velocity with a mean of zero m/s and a standard deviation of 1.4 x 10^4 m/s in each of r, phi and z directions. The r-direction is taken as the radial distance from the axis of symmetry, the phi-direction is perpendicular to the 2D axisymmetric representation of the ECR ion source and the z-direction is along the path of the beam. The velocity distribution was based on a proton energy of 1 eV.

$$E = \frac{1}{2} m_p v_p^2 \qquad \textbf{eq. 4.1}$$

$$1\ eV \cdot 1.6 \cdot 10^{-19} \frac{J}{eV} = \frac{1}{2} m_p v_p^2$$

$$v_p = 1.4 \times 10^4 \frac{m}{s}$$

4.2. Analyzing Beam Simulation

The particle tracing code within COMSOL provides visualizations of the beam profile such as the one show in Figure 4.3. COMSOL does not provide tools for beam simulation analysis, such as emittance or particle distribution. In order to analyze the beam simulation several post processing tools were developed in MATLAB as part of this work.

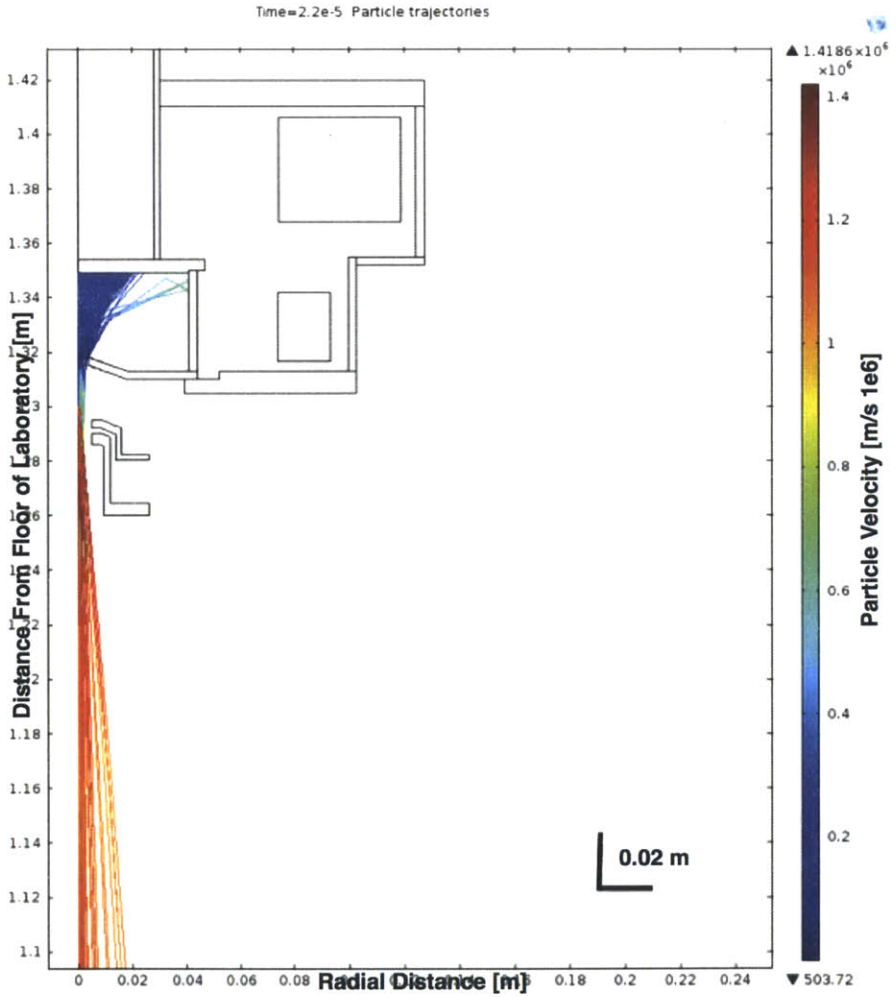

Figure 4.3 – Axisymmetric cylindrical cross section of the ECR ion source showing the simulated beam profile using COMSOL Charged Particle Tracing code with the highest total particle speed regions in red, 1.4 x 10^6 [m/s]

4.3. Plotting Emittance

COMSOL Charged Particle Tracing code can output a csv file from beam simulation comprised of particle locations and velocities in two dimensions. The csv file from COMSOL can be imported into MATLAB and manipulated as a large matrix. In order to visualize the beam simulation, a 2mm wide radial slice of particle simulation data was selected for analysis. Emittance and particle distribution plots were generated using tools written in MATLAB.

Emittance plots in phase space, v_r/v_z, provide information about the rate of spread of the beam and Cumulative Density Function, CDF, plots provide information about the spread of the beam particles. The emittance ellipse provided with the phase space plot is a two-sigma emittance ellipse, meaning it encompasses 95% of the beam particles.

Figure 4.4 and 4.5 demonstrate the tools developed to analyze the characteristics of the beam returned by simulation. The emittance plot shown in Figure 4.4 is from a simulation of a 10kV extraction electrode and a plasma meniscus with a concave minor radius of 0.5mm. The slice of beam data was taken 16cm below the extraction electrode, or 1.15m above the floor of the laboratory. This location is

significant because it is the location of the beam current measurement device used to test the performance of the ECR ion source.

The emittance plot in Figure 4.4 shows the beam is diverging because it tilted with a positive slope. Even though the beam is diverging, almost 90% of the simulated beam is located within a 1cm radius, shown by the particle CDF in Figure 4.5. The simulated particle distribution indicates that the beam has a small radius 16cm below the extraction electrode but the beam will spread rapidly further along the beam path. The beam drift distance of 16cm is used because it is the location of the beam current measuring device described in section 5.

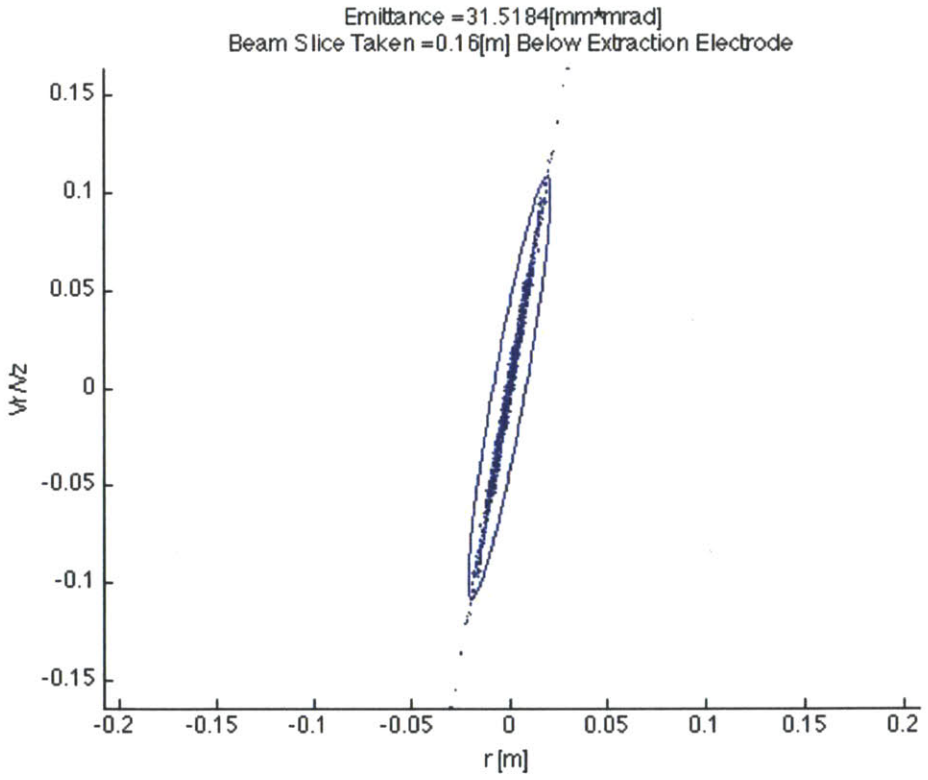

Figure 4.4 – Emittance ellipse showing 2mA beam simulation extracted at 10kV from a 0.5mm concave minor radius meniscus. The simulated beam slice is taken at location of the beam current measuring device described in section 5, 16cm below the extraction electrode

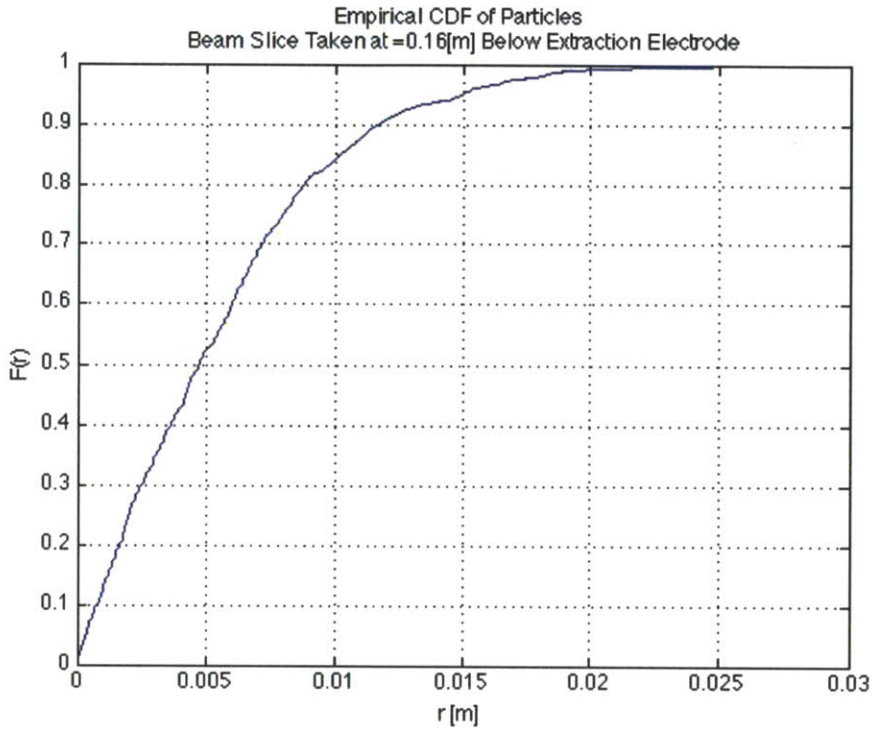

Figure 4.5 – CDF showing 90% of simulated beam within 1cm radius. The particle distribution is calculated from 2mA beam simulation extracted at 10kV from a 0.5mm concave minor radius meniscus. The simulated beam slice is taken at location of the beam current measuring device described in section 5, 16cm below the extraction electrode

5. Beam Current Measurement

This section describes the instruments used to measure the beam current of an ECR ion source. The design of the beam current measuring device used to test the performance of the ECR ion source as part of the test assembly at MIT is also presented.

5.1. Faraday Cup with Secondary Electron Capture

A Faraday cup is one of the most common instruments used to measure beam current. The plates of a Faraday cup intercept a charged particle beam as shown in Figure 5.1. Beam current is measured by connecting these plates to ground. The sides of a Faraday cup serve to capture electrons from secondary emission.

As high energy positively charged particles impact the plates of the Faraday cup, secondary electrons are emitted. If these electrons are not captured on the plates or walls of the Faraday cup, by charge balance, they appear as the collection of additional positive ions, overestimating the intercepted beam current.

In order to capture the electrons emitted from the beam striking the plates of the Faraday cup, a static magnetic field can be used perpendicular to the path of secondary electrons exiting the Faraday cup. The magnetic field strength must be sufficiently large to limit the electron cyclotron radius of the secondary electron so they are not able to escape the Faraday cup. By capturing all of the positively

charged particles from the beam and all of the electrons created by secondary emission, the Faraday cup is able to accurately measure beam current.

Secondary electrons are emitted with energy of about 10 eV. In order to limit the electron cyclotron radius to 1 cm a magnetic field of at least $3.4 \cdot 10^4$ tesla is required. A magnetic field of this strength does not significantly effect the path of a proton entering the Faraday cup at 10keV because the proton is much more massive. A proton cyclotron radius of 1cm would require a magnetic field over three orders of magnitude larger.

$$\frac{qB}{m} = \frac{v}{r}$$

$$B = \frac{vm}{qr}$$

$$\frac{qB}{m} = \frac{v}{r}$$

$$\frac{B_{proton}}{B_{electron}} = \frac{m_p v_p}{m_e v_e}$$

$$10\ keV\ proton\ and\ 10\ eV\ electron$$

$$\frac{B_p}{B_e} = 1.4 \cdot 10^3$$

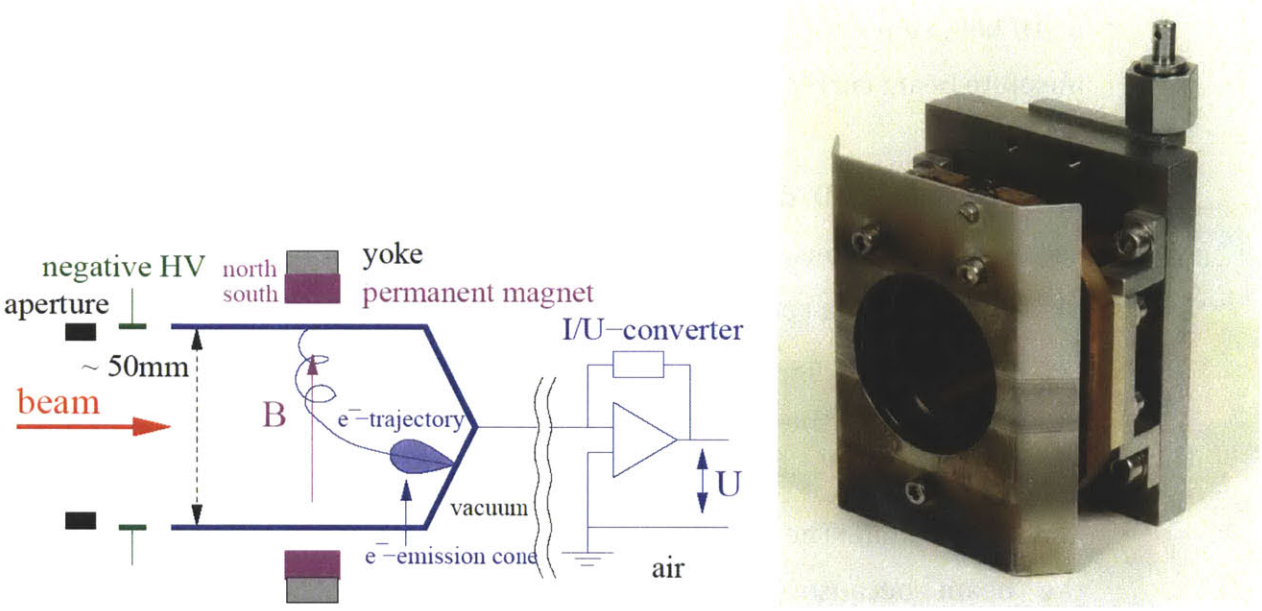

Figure 5.1 – Faraday cup with magnetic secondary electron capture

5.2. Beam Current Measuring Device

This section describes the Current Measuring Device, CMD, designed to measure the beam current of the ECR ion source presented in the earlier sections of this thesis. The CMD is based on the same principle as a Faraday cup but it has two main differences.

The current measuring device does not have a mechanism, such as a transverse magnetic field, to capture electrons released by secondary particle emission. Without proper capture of secondary electrons, the current measuring device will overestimate the beam current but it should still be able to measure positive beam current if it is impacted by a positively charged particle beam. Based on literature, secondary electron emission yield is less than 1 for protons

at 10 keV, so we expect this to introduce at most a factor of two uncertainty in absolute beam current measurement from the CMD.

Although the CMD does not maintain proper charge balance by capturing secondary electrons, it will provide more information about the particle distribution than a conventional Faraday cup. The current measuring device is divided into sections, shown in Figure 5.3, made of copper. Each section of the Faraday plate on the CMD is electrically isolated from the positioning piston and each other. Electrical isolation is achieved with boron nitride bolt sleeves and Kapton film. The sections provide insight into the particle distribution of the beam because they can be measured independently. The particle distribution information measured with the current measuring device will compared with simulation to determine the concavity of the plasma meniscus.

The center section of the current measuring device has a radius of only 1cm while the four outer sections are 4cm wide, shown in Figure 5.3. The ratio of the particles located on the center section of the plate compared to the outer sections should provide enough information about the spread of the beam to indicate the shape of the plasma meniscus. Once the shape of the plasma meniscus is established, high field axial cyclotron injection from the ion source can be simulated with more confidence.

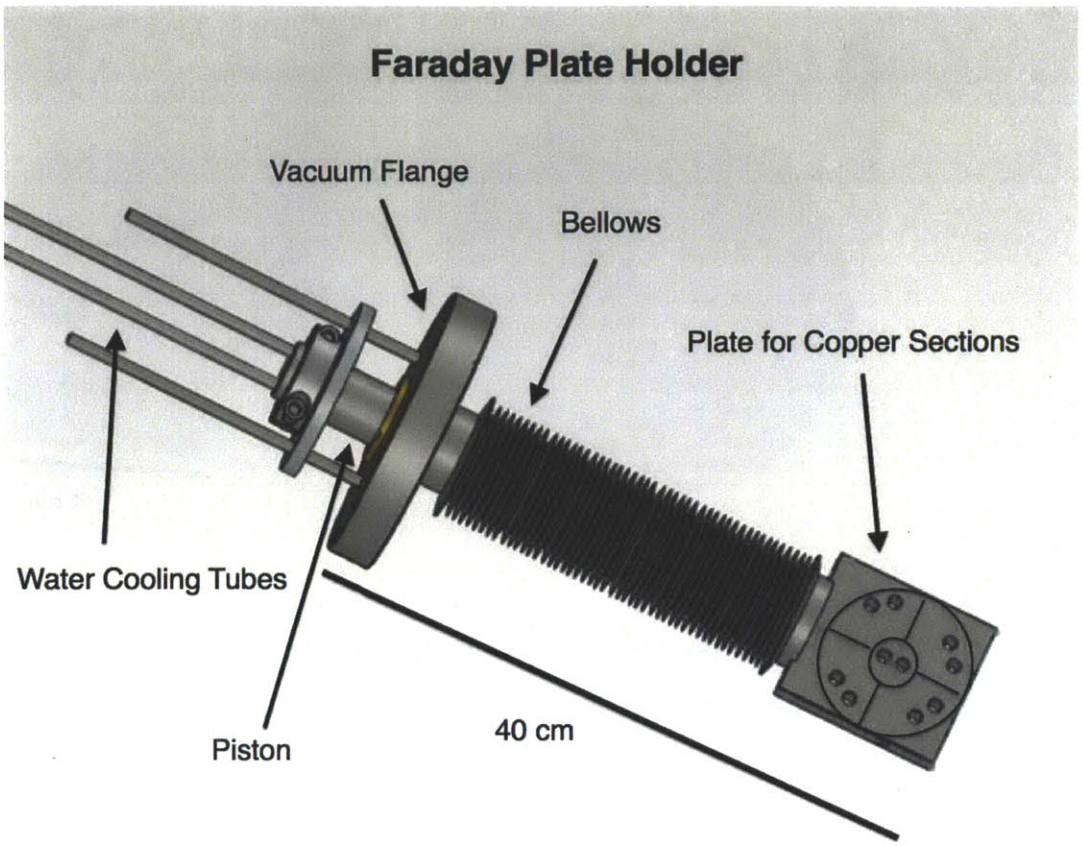

Fig. 5.2 – Faraday Plate Holder. The holes on the plate provide mounting for the copper sections, they have suffiecnt clearance to allow boron nitride bolt sleves

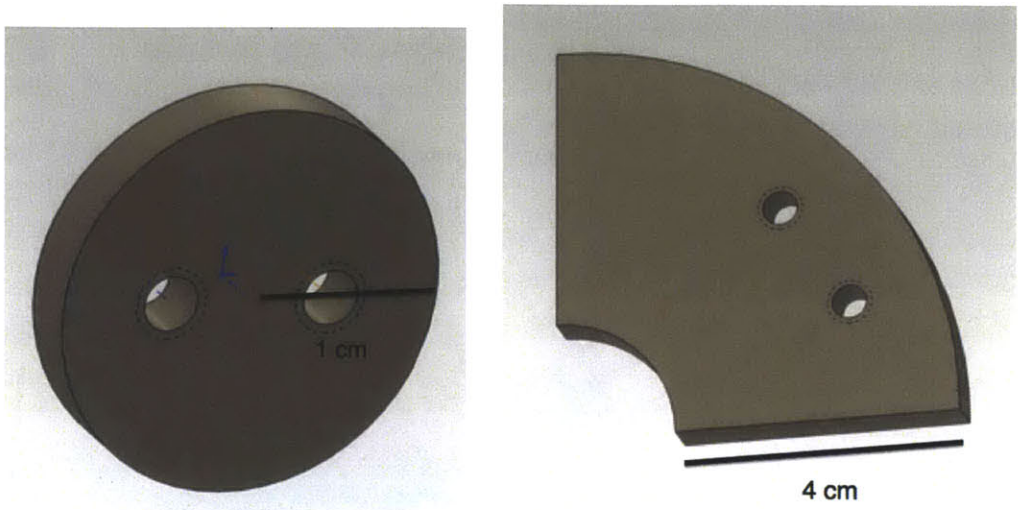

Fig. 5.3 – Center and outer copper sections of Faraday Plate. The copper section on the right is one of 4 that surrond the smaller center section shown on the left

5.2.1. Beam Power

If the extracted beam current were large enough, it might be possible to overheat the copper or some of the electrical insulating material that compose the plate of the beam current measuring device. The calculation below provides insight into the necessity for water cooling of the beam current measuring device. A high intensity beam operating at 20mA and 20keV produces a power of 400 Watts. With 400 watts of power overheating could be a concern. A more modest beam output of 5mA at 10keV produces a beam power of only be 50 watts. In order to be certain

of the temperature of the current measuring device and avoid overheating in the case of unexpectedly larger beam current, thermocouple wire was attached to the center section providing temperature monitoring.

$$H^+ \text{ @ } 2mA \text{ and } 10kV$$

$$N = \frac{I}{q} \quad \left[{particles}/{s}\right]$$

$$\mathrm{N} = \frac{20 \cdot 10^{-3} \frac{\mathrm{C}}{s}}{1.6 \cdot 10^{-19} \frac{C}{particle}}$$

$$N = \ 10^{17} \frac{particles}{s}$$

$$P_{Beam} = \mathrm{N} \cdot E_p \left[\frac{J}{s}\right]$$

$$P_{Beam} = 10^{17} \frac{particles}{s} \cdot 1.6 \cdot 10^{-19} \frac{J}{eV} \cdot 2 \cdot 10^4 eV$$

$$P_{Beam} = 400 \, Watts$$

6. Emittance Measurement

This section describes the design of a pepper pot emittance measuring device using a thallium doped cesium iodide scintillator, CsI:Tl, to visualize beam spread and measure emittance through a clear window.

6.1. Emittance Measurement Technique

A "pepper pot" emittance device collimates the beam into small beamlets of known radius allowing the spread of the beam for a given distance to be visualized. Figure 6.1 illustrates this technique.

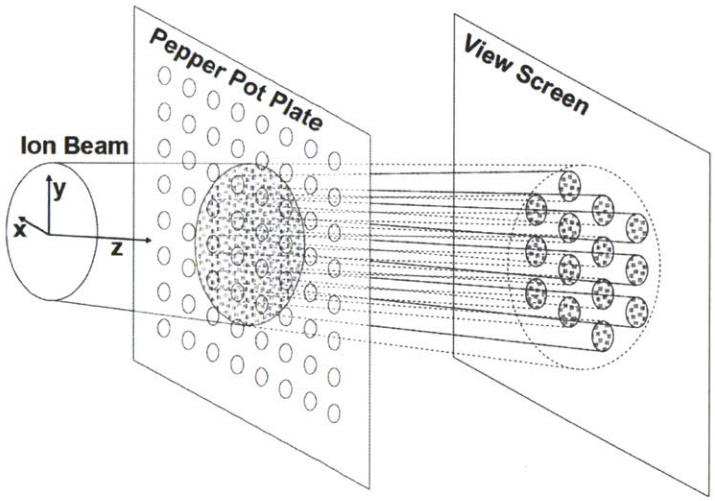

Figure 6.1 Basic principle used to visualize emittance using a pepper pot [24]

6.2. Thallium Doped Cesium Iodide Scintillators

Thallium doped Cesium Iodide scintillators, CsI:Tl, are more attractive than typical phosphorus based scintillators due to their greater light output at low beam energies. The number of photons emitted from CsI:Tl scintillator scales with the energy of the incident proton. For incident protons between 50 keV and 200 keV, the number photons emitted from CsI:Tl scintillator has been experimentally shown to vary linearly with energy, 200 keV protons were shown to emit 4 times more photons than 50 keV protons at a ratio of 60,000 photons/MeV **[10]**. The photons emitting from CsI:Tl scintillator are of 550nm wavelength, within the visible spectrum. For the purpose of this design, it is assumed that this linear photon to particle energy relationship will scale to proton energies within the range of the ECR ion in this thesis, 20 keV.

Beams with beam current corresponding to 10^6 particles per second have been visualized with CsI:Tl scintillator. The beam produce by the ECR ion source will have a far greater particle incidence rate. A proton beam of 10 mA produces 10^{17} particles per second, at this beam current a CsI:Tl scintillator would produce 10^{20} photons per second. Using the calculation below, the power output of the light from the CsI:Tl scintillator would exceed 3 Watts/steradian. 3 Watts/steradian of power output in the visible spectrum should be more than adequate to visualize the beam from the ECR ion source, especially under dark conditions.

$$10\ mA\ proton\ beam\ at\ 20\ keV$$

$$10^{17}\frac{particles}{s} = \frac{10^{-2}\frac{C}{s}}{10^{-19}\frac{C}{particle}}$$

$$10^{20}\frac{photons}{s} = 10^{17}\frac{particles}{s}\cdot 10^{3}\frac{photons}{particle}\cdot$$

$$3\frac{Watts}{sr} = 10^{20}\frac{photons}{s}\cdot 2\frac{eV}{photon}\cdot\frac{1.6\cdot 10^{-19}\frac{J}{eV}}{4\pi\ sr}$$

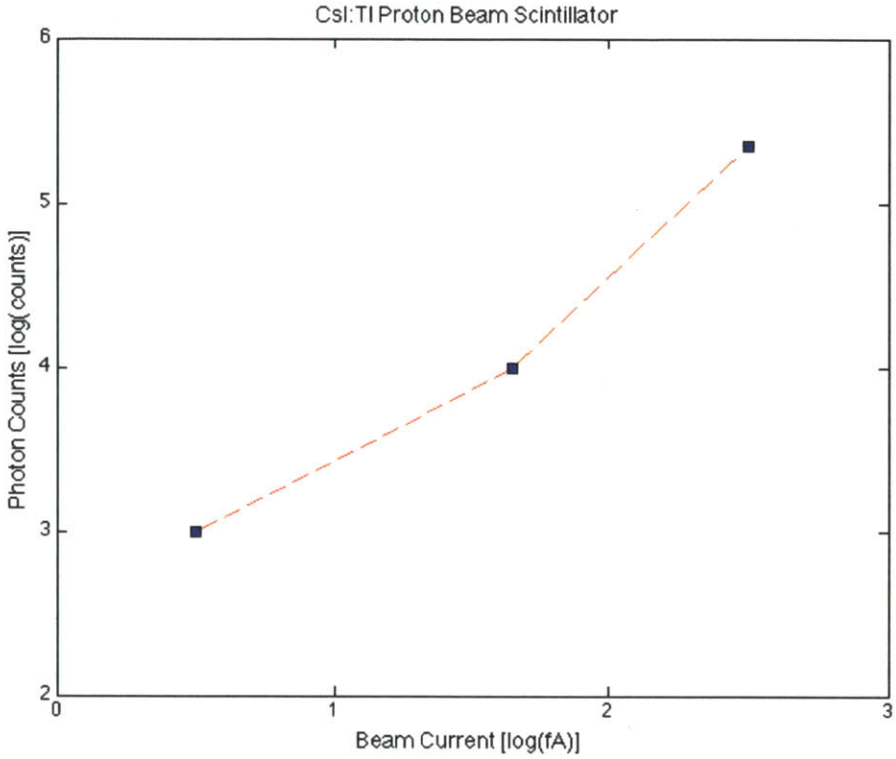

Figure 6.2 – Photon counts of CsI:Tl scintillator for use in low intensity, fA, proton beams at 50keV [9]

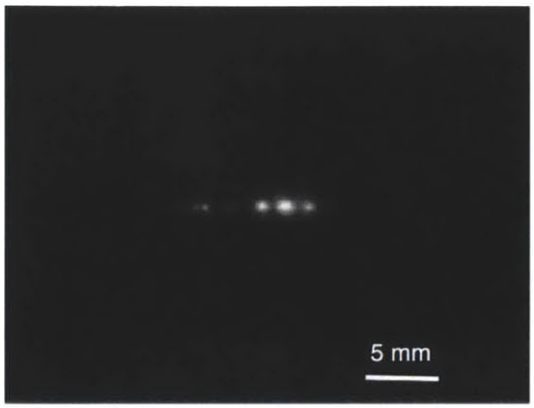

Figure 6.3 – Light from CsI:Tl scintillator and low intensity proton beam, 1 fA at 200 keV [9]

6.3. CsI:Tl Scintillator Pepper Pot Design

The CsI:Tl scintillator pepper pot emittance measuring device outlined in this section is sized for placement 76cm from the extraction electrode of the ECR ion source. This location is representative of the central accelerating plane of a high field compact superconducting cyclotron suitable for proton therapy. The design is also flexible enough that it could also be placed below the superconducting magnet in the test configuration at MIT, a beam drift distance of close to 90 cm, shown in Figure 7.1. Placing the CsI:Tl pepper pot below the beam pipe traveling through the superconducting magnet would allow for an emittance measurement from the ECR ion source with only moderate modifications to the MIT test configuration.

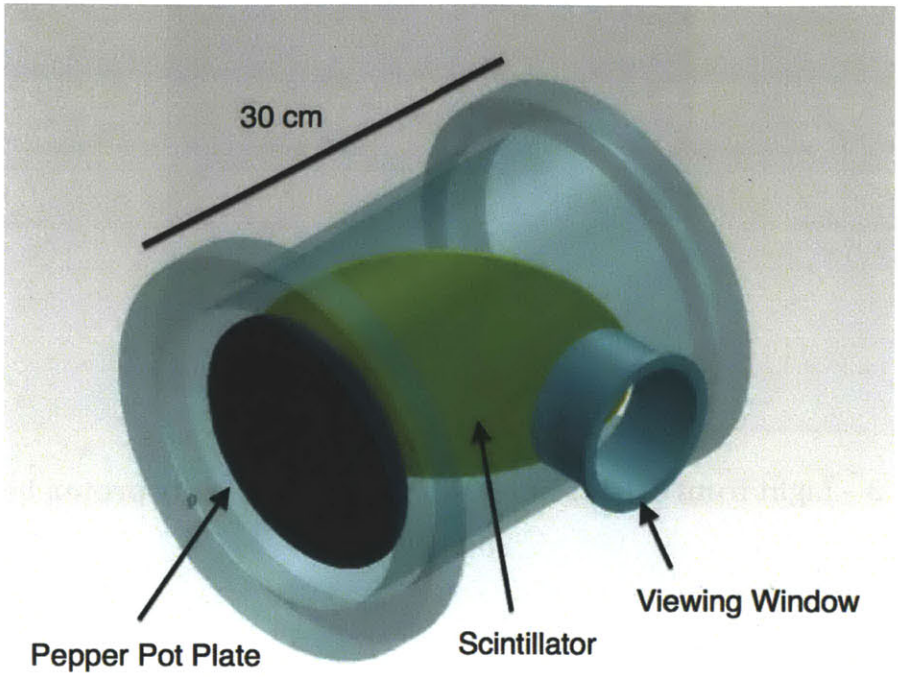

Figure 6.4 – Pepper pot plate and 45° tilted CsI:Tl scintillator

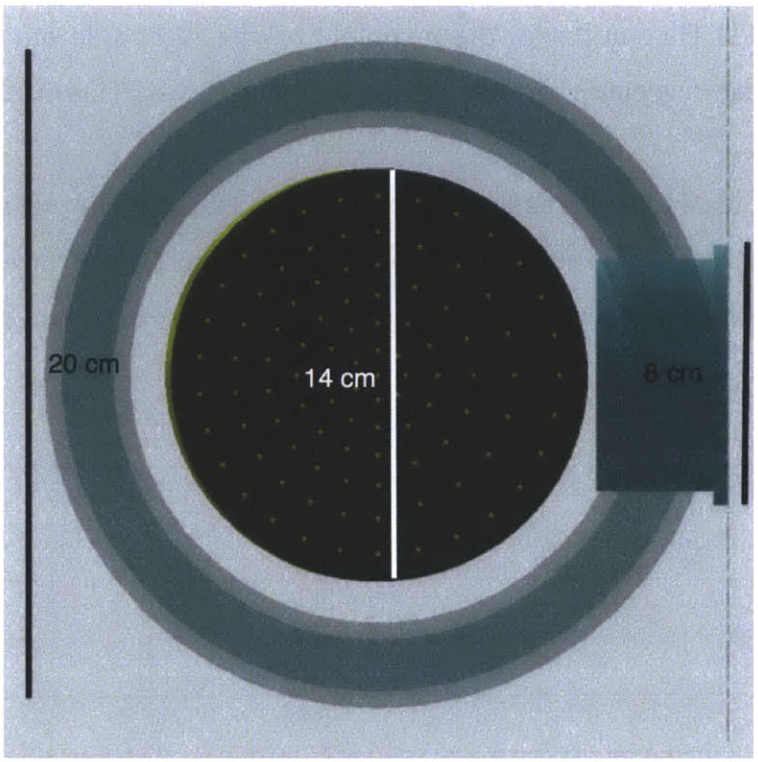

Figure 6.5 - Pepper pot plate with holes spaced to prevent beamlet overlap

6.3.1. Pepper Pot Collimation from Beam Simulation

The scintillating screen of the CsI:Tl pepper pot is tilted to allow viewing through the adjacent window. Figure 6.5 displays the variation in the radial spacing of the holes in the pepper pot plate. This variation allows the maximum number of 2mm diameter holes without allowing the beamlets to overlap on the CsI:Tl scintillator. On the right hand side of the pepper pot screen in Figure 6.5 the holes are spaced further apart than on the left. This is the effect of the

tilted CsI:Tl scintillator, the beamlets on the right side have further to travel resulting in greater spread before impacting the CsI:Tl scintillator.

The holes have increasing radial spacing because the radial velocity on the outer edge of the beam is larger than near the center. From simulation of a 2mA proton beam extracted at 10kV at r = 2cm, v_r = 0.01 m/s but at r= 4cm, v_r= 0.04 m/s.

Near Side (left) – radius [mm]	Far side (right) – radius [mm]
9	10
19	21.5
29	34.5
46	49
52	65
65	

Figure 6.6 – Radial location of holes in pepper pot collimator

Figure 6.7 and 6.8 display the resulting emittance plots generated by a simulation of the CsI:Tl pepper pot design for beam drift distances of 16cm and 76cm below the extraction electrode. These locations correspond to the beam current measuring device and accelerating plane of a compact cyclotron. The beam data is taken from simulation and collimated to reflect the hole pattern in Figure 6.5. Notice the emittance ellipse area near the extraction electrode is 45 $mm \cdot mrad$, while further down the beam path the emittance ellipse area is

only 20 $mm \cdot mrad$. This drastic difference in emittance ellipse area shows that the beam is spreading rapidly close to the extraction electrode. Although the rate of beam spread has decreased once it has traveled 76cm, the location of the cyclotron mid-plane, the beam is spread much further radially, extending to 5cm, and it not likely to be suitable for injection into the cyclotron.

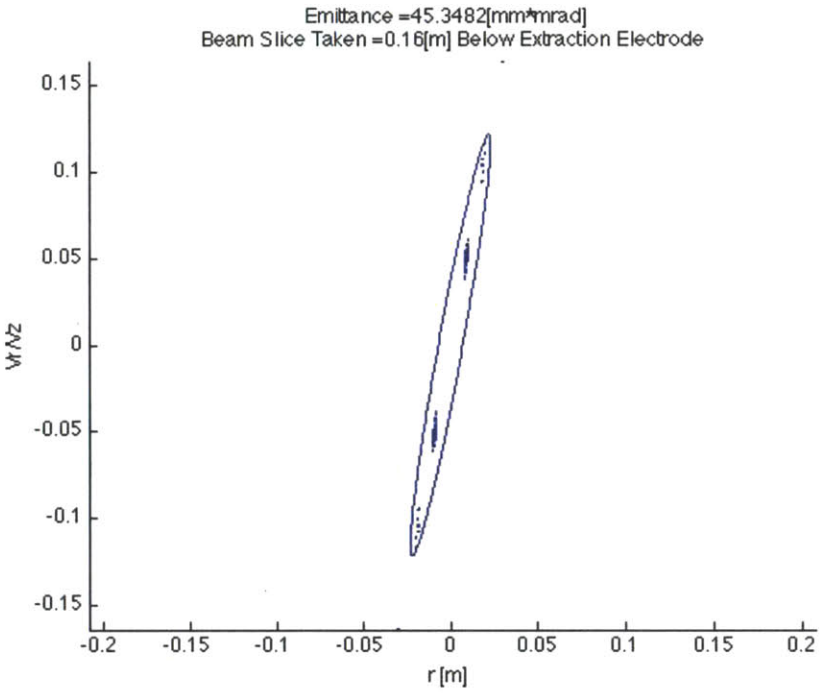

Figure 6.7 – Emittance plot with simulated pepper pot. The 2 mA beam was collimated 16 cm below the extraction electrode with energy of 10 keV and 0.05 mm concave plasma meniscus minor radius

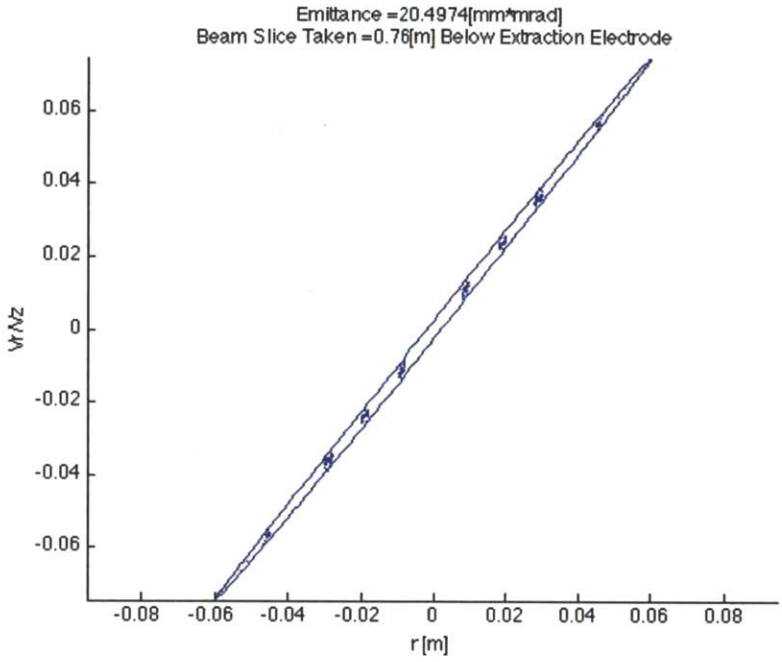

Figure 6.8 – Emittance plot with simulated pepper pot. The 2 mA beam was collimated beam 76 cm below the extraction electrode with energy of 10 keV and 0.05 mm concave plasma meniscus minor radius

7. ECR Performance Data

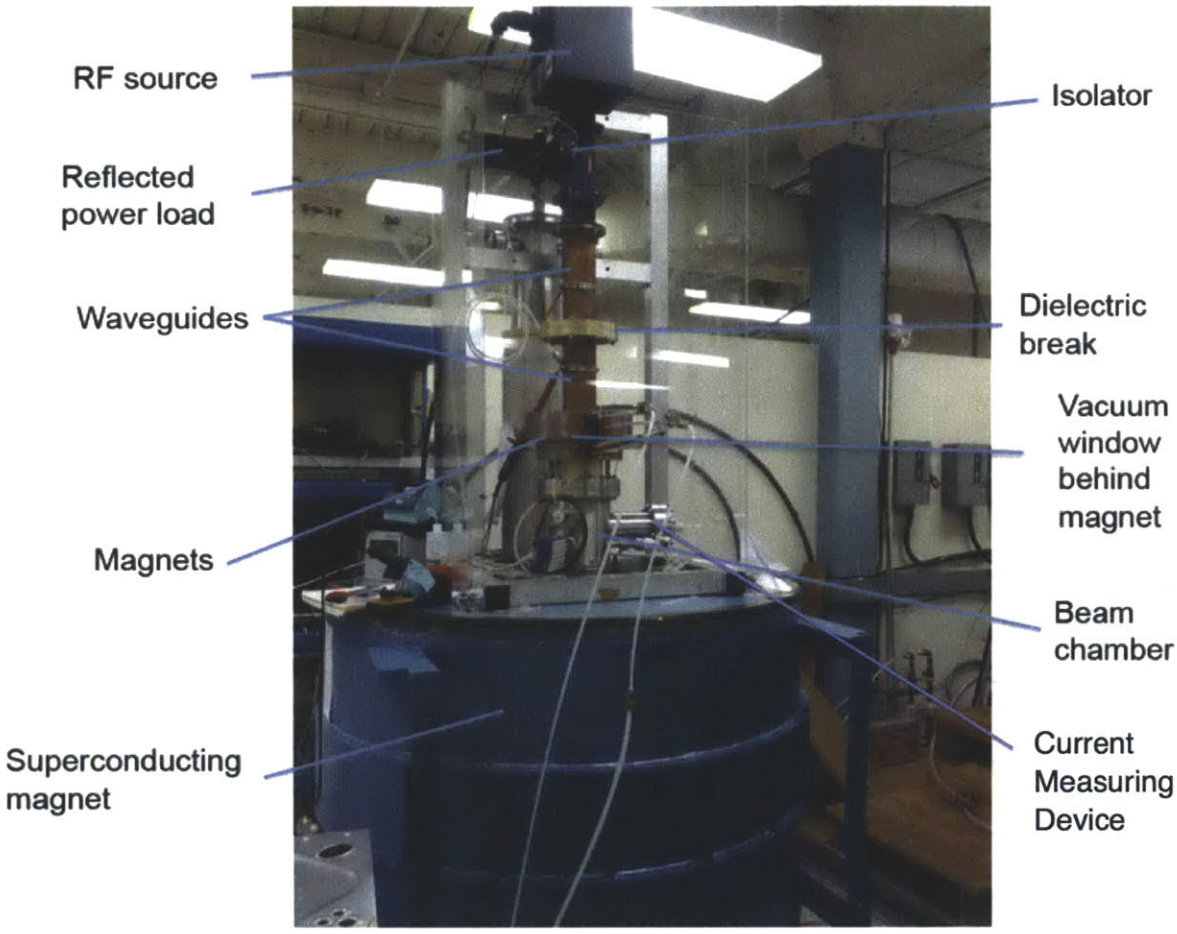

Figure 7.1 – MIT ECR Ion Source Test Configuration

7.1. Experimentally Measured Beam Current

The ECR Ion Source described in this thesis was able to produce a positively charged particle beam with a maximum measured beam current of 0.72 mA at an

extraction voltage of 10kV. The plasma was achieved and beam was extracted with current of 203 amps and 43.6 amps in the upper and lower ion source coils. A flow rate of 10 scc/min of high purity hydrogen gas was fed into the ion source with a forward microwave power of 95 watts and a reflected power of 65 watts. The vacuum pressure was $5x10^{-5}$ mBar with zero gas flow and during operation the pressure increased to $5x10^{-3}$ mBar. The maximum extraction voltage achieved was 10kV before arcing from the high voltage components to the ground components occurred.

The low microwave power and low quality vacuum were probably the most significant factors limiting the beam current extracted from the ion source. In order to produce a beam with power on the order of 400 Watts requires an even greater amount of input power from the microwave source. The microwave system safety protection was triggered repeatedly when trying to achieve higher output power and thus had to be limited during the ion source test. The microwave window directly above the plasma chamber of the ion source was a significant source of vacuum leak during assembly and had to be sealed with flexible epoxy. Ultimately the microwave window leak limited the vacuum quality in the ion source. Higher pressure in the plasma chamber causes increased recombination of plasma ions reducing the number of positive ions available for extraction and the beam current from the ion source. An increase in microwave power and an improved vacuum quality would likely significantly increase the beam current extracted from the ion source.

During the experiment, only the center section of the beam current measuring device was able to register beam current. This result is not unexpected given the close proximity of the beam current measuring device, 16cm, to the extraction

electrode aperture of diameter 8mm. The beam current measurement still provides insight into the shape of the plasma meniscus. Figure 7.3 describes the beam current measured during the MIT test using the current measuring device.

Upper ECR solenoid current	203 amps
Lower ECR solenoid current	43.6 amps
Hydrogen gas flow rate	10 scc/min
Forward microwave power	95 Watts
Reflected microwave power	65 Watts
Vacuum pressure during test	$5x10^{-3}$ mBar
Maximum extraction voltage	10 kV
Maximum beam current	0.72 mA

Figure 7.2 – ECR ion source operating parameters during MIT test

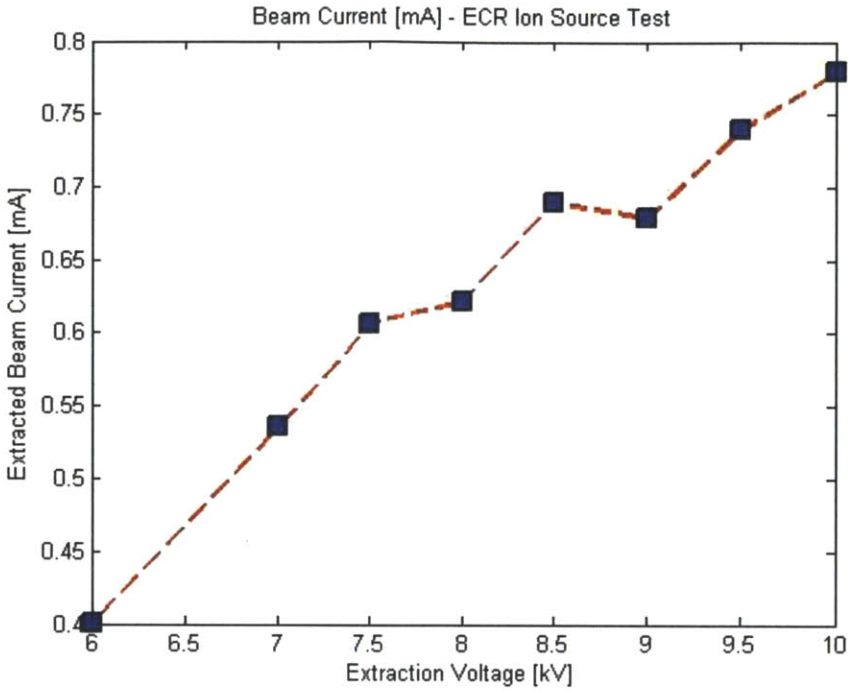

Figure 7.3 – Beam Current Measured During MIT ECR Test

7.1.1. Determining the Plasma Meniscus Shape

When comparing the measured beam current distribution with simulations of various plasma meniscus shapes, only the concave surfaces have a significant fraction of the particle distribution within a 1 cm radius a distance of 16cm from the extraction electrode, the location of the center section of the current measuring device. Based on simulation of various plasma meniscus shapes, Figure 7.4, a concave plasma meniscus is the only surface consistent with a beam current measurement exclusively on the center section of the beam current measuring device.

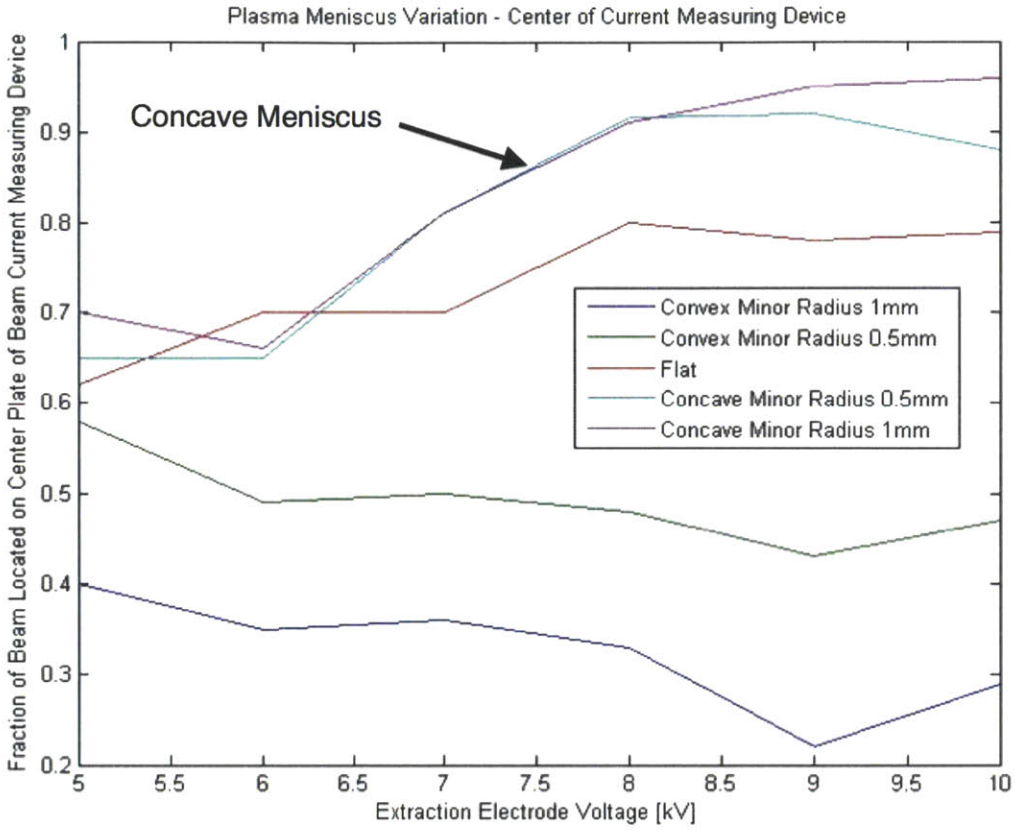

Figure 7.4 – Particle distribution for varying plasma meniscus concavity and minor radius shapes. This plot is based on simulations of 2mA proton beams.

7.2. Beam Injection into High Field Compact Cyclotron

With confidence in the shape of the plasma meniscus one can simulate axial injection into a high field cyclotron.

7.2.1. Simulation of Beam Injection into Compact Cyclotron

Figure 7.6 shows the magnetic field of an axisymmetric cross section from a preliminary design of a compact cyclotron. Although this beam simulation is conducted at 4 tesla and would not allow full acceleration of protons to 230 MeV, 4 tesla is sufficient field strength to indicate if higher field injections are plausible. Figure 7.5 displays the beam profile of a 2mA 10 keV beam injected into a compact cyclotron. It is clear from the beam profile and particle distribution, Figure 7.6, the beam spread is too large to successfully bend into the accelerating plane of the cyclotron. Figure 7.6 shows that only 40% of the beam is within a 1cm radius. Ultimately, this beam simulation suggests the performance of the ion source should be improved before high field cyclotron injection is revisited.

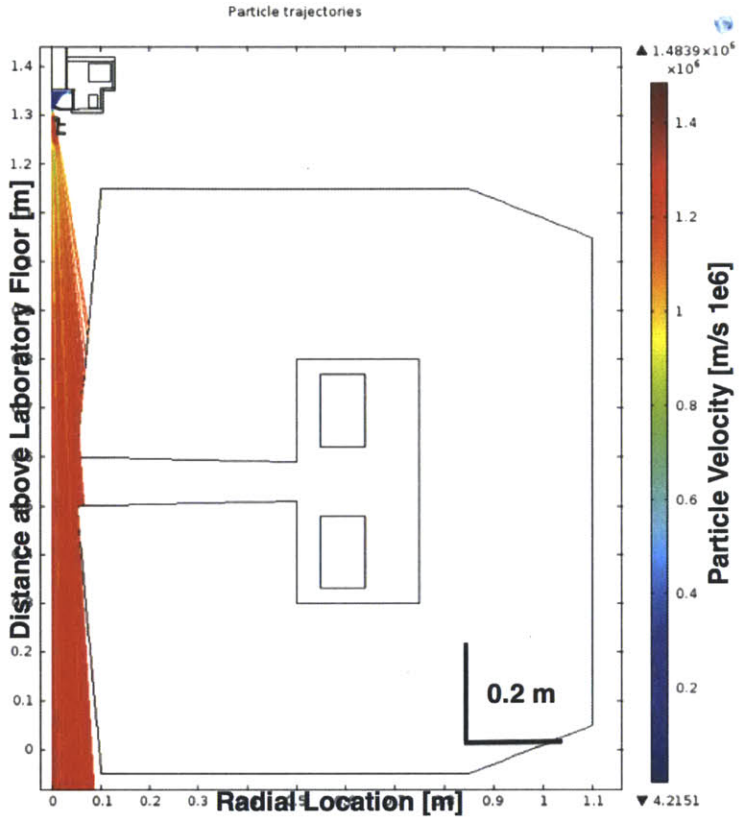

Figure 7.5 – Axisymmetric cylindrical cross section of beam profile showing axial injection into 4T Cyclotron with 10kV extraction voltage and 2mA beam current

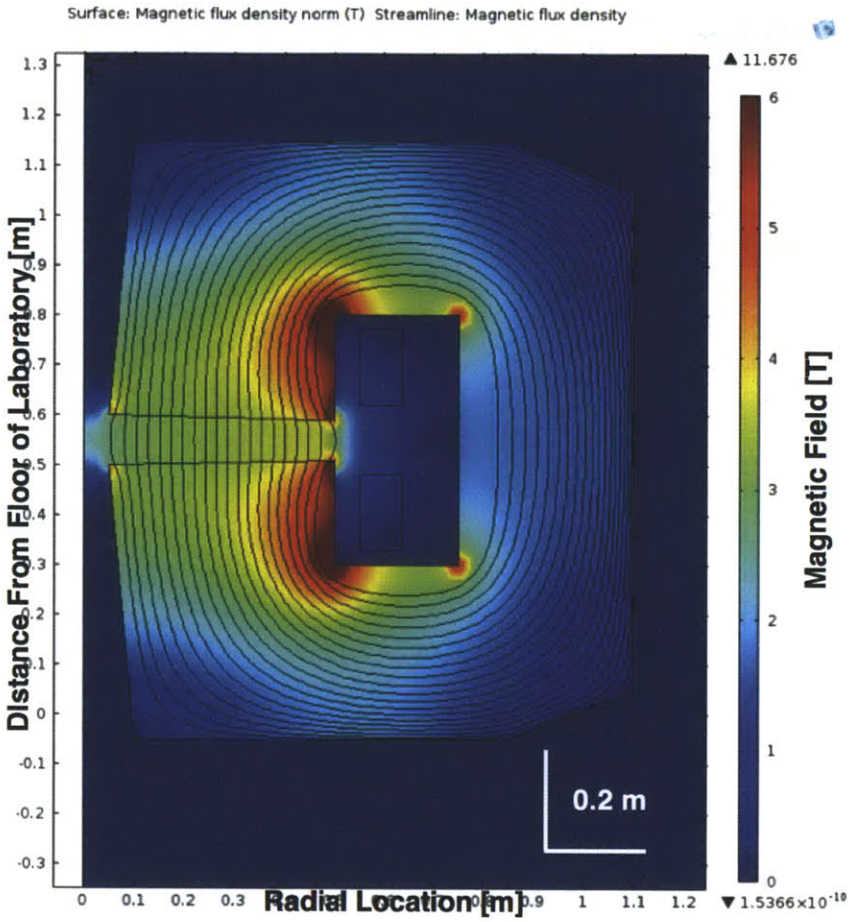

Figure 7.6 – Axisymmetric cylindrical cross section. Compact cyclotron magnetic field

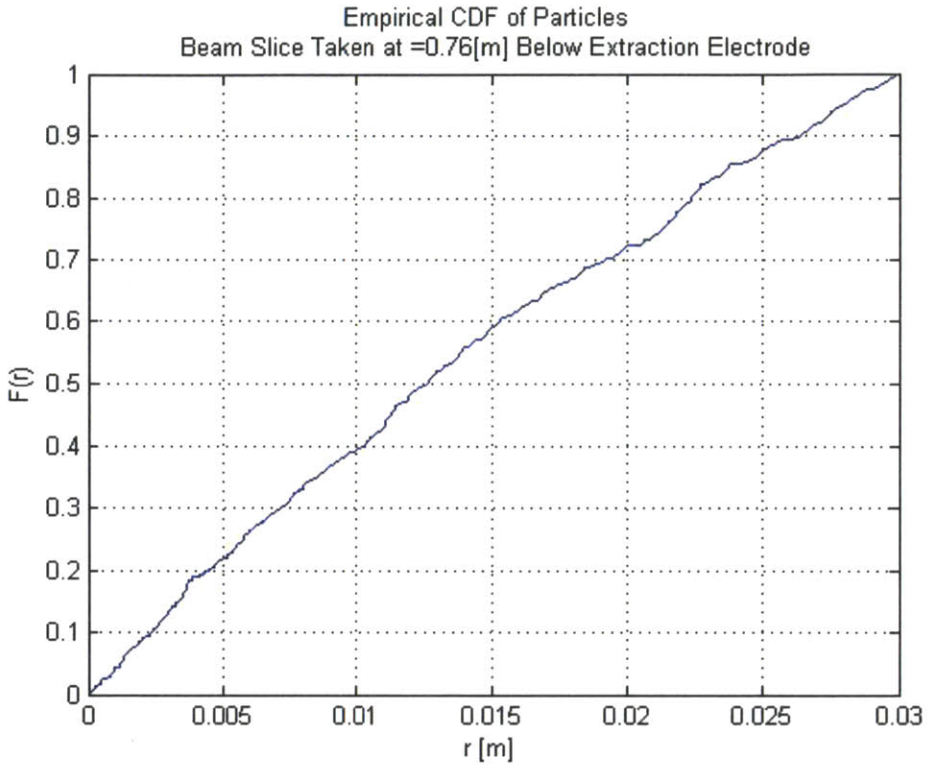

Figure 7.7 – Particle distribution of simulated beam slice taken at 76cm below the extraction electrode, the location of the center plane of the cyclotron. Beam is simulated as 2mA, extracted at 10kV. Cyclotron field of 4T.

7.3. Closing Remarks

Although the ion source test was successful to the extent that a positively charged particle beam was extracted and measured, the ion source operating parameters still need to be manipulated to improve its performance. These parameters include the

current in the solenoid coils, hydrogen gas flow rate, microwave power, vacuum pressure and extraction voltage.

It would be preferable to have a vacuum quality on the order of 10^{-6} mBar. An improved vacuum could reduce plasma ion recombination and increase the extracted beam current. It may also be useful to measure the extracted ion species by using a dipole bending magnet mass spectrometer to determine the optimal gas flow rate. The different ion species could be viewed on a Cesium Iodide scintillator similar to the one described in section 6.

The available power output from the microwave system must be increased drastically to achieve the desired beam current from the ECR ion source. This may require a microwave system with available power output exceeding 1 kW.

During testing the extraction voltage was limited by arcing between the high voltage components and the solenoid coils which were held at ground potential. In order to increase the extraction voltage one could coat the inside of the iron shroud in a thick layer Teflon or design an insulating housing for the ECR solenoid coils.

The beam current measuring device should be replaced with a Faraday cup that accurately measures beam by capturing secondary electrons. Once a measured beam current of 10 mA has been exceeded, detailed emittance measurements should be taken with the Cesium Iodide scintillator pepper pot described in section 6.

Once satisfactory performance of the ion source has been established with reliable beam current and extraction voltage one could redesign the extraction electrode angle to take into account the concave plasma meniscus and provide focusing to match the

spreading of the beam due to space charge. A beam code that calculates space charge forces discretely from each surrounding particle should be explored for higher beam current simulations. Beam3D is a code developed at Michigan State University in the late 1980s for ion source beam transport simulations with this type of space charge calculation. In order to complete beam simulations reliably for varying plasma meniscus shapes Beam3D would require modernization but would be a worthwhile effort.

For the long path length required for axial injection into a cyclotron, additional focusing magnets, possibly small permanent quadrupole magnets, could also be explored. Small quadrupole magnets could be preferable to modifying the extraction electrode geometry to match space charge effects, which vary with beam current.

Ultimately, with some design improvements and changes to the operating parameters, it could be possible to extract over 10mA of beam current at 20kV from this ion source with adequately small beam spread for axial injection into a cyclotron but further investigation is required.

References

[1] Antaya, T. A., L. Bromberg, R. C. Lanza, and J. V. Minervini. *Frontier Studies of Single Stage Superconducting Cyclotron-based Primary Accelerators for Topic I: Sensing Fissile Materials at Long Range*. Massachusetts Institute of Technology, Cambridge, MA.

[2] Antaya, Timothy. "There Are 3 Kinds of Cyclotrons." Comprehensive Intro to Cyclotron Science and Technology. United States, Cambridge, MA. 15 Jan. 2011.

[3] Batygin, Y., A. Goto, and Y. Yano. "NONLINEAR BEAM DYNAMICS EFFECTS IN HEAVY ION TRANSPORT LINE." *The Institute of Physical and Chemical Research (RIKEN)*

[4] Cawthron, E. R. "Secondary Electron Emission from Solid Surfaces Bombarded by Medium Energy Ions." *Australian Journal of Physics* 24 (1971): 859

[5] Dattoli, G., E. Sabia, M. D. Franco, and A. Petralia. *Slices and Ellipse Geometry*. Thesis. ENEA

[6] Farr, J. B., A. E. Mascia, W.-C. Hsi, C. E. Allgower, F. Jesseph, A. N. Schreuder, M. Wolanski, D. F. Nichiporov, and V. Anferov. "Clinical Characterization of a Proton

Beam Continuous Uniform Scanning System with Dose Layer Stacking." *Medical Physics* 35.11 (2008): 4945.

[7] Guharay, S. K., M. Hamabe, and T. Kuroda. "A Novel Ion Beam Monitor Using Kapton Foils." *Review of Scientific Instruments* 69.5 (1998): 2182.

[8] Halbach, K., and R. F. Holsinger. "SUPERFISH - A Computer Program for Evaluation of RF Cavities with Cylindrical Symmetry." *Particle Accelerators 7* (1976): 213-22

[9] Haouat, G., N. Pichoff, P. Y. Beauvais, and R. Ferdinand. "Measurements of Initial Beam Conditions for Halo Formation Studies." *International Conference on Ion Sources* (2009)

[10] Harasimowicz, Janusz, Luigi Cosetino, Paolo Finocchiaro, Alfio Pappalardo, and Carsten Welsch. "Scintillating Screens Sensitivity and Resolution Studies for Low Energy, Low Intensity Beam Diagnostics." *Review of Scientific Instruments* 81.103302 (2010)

[11] Humphries, Stanley. *Principles of Charged Particle Acceleration*. New York: J. Wiley, 1986.

[12] Inouchi, Yutaka, Shohei Okuda, Hideki Fujita, Yoshitaka Sasamura, and Masao Naito. "BEAM CURRENT CONTROL OF AN ECR ION SOURCE FOR MEDIUM CURRENT ION IMPLANTER." *High Technology Research and New Business Division, Nissin Electric Co., Ltd.,* (1999)

[13] Iwasa, Y. "Magnets & Field II." Course 2.64 Lecture 5. Massachusetts Institute of Technology, Cambridge, MA. 15 Feb. 2011.

[14] Jolly, S., J. Pozimski, and P. Savage. "Beam Diagnostics for the Front End Test Stand at RAL." *Proceeding of DIPAC* (2007): 218-20.

[15] Jolly, S., J. Pozimski, J. Pfister, and O. Kester. "Data Acquisition and Error Analysis for Pepperpot Emittance Measurements." *Proceedings of DIPAC09* (2009): 1-3.

[16] Kashiwagi, H., T. Hattori, M. Okamura, Y. Takahashi, T. Hata, K. Yamamoto, S. Okada, and T. Sugita. "Design and Construction of Four-hole ECR Ion Source." *Review of Scientific Instruments* 73.2 (2002): 583-85.

[17] Krane, Kenneth S., and David Halliday. *Introductory Nuclear Physics*. Cyclotron Accelerators. 571-581. New York: Wiley, 1988.

[18] Law, W. M., C. D. Levy, and P. W. Schmor. "Emittance and Brightness Measurements in a Proton Electron Cyclotron Resonance Ion Source." *Nuclear Instruments and Methods in Physics Research* A290 (1990): 308-14.

[19] Lawrie, S. R., D. C. Faircloth, A. P. Letchford, C. Gabor, and J. K. Pozimski. "Plasma Meniscus and Extraction Electrode Studies of the ISIS H− Ion Source." *Review of Scientific Instruments* 81 (2010)

[20] Lieberman, M. A., and Allan J. Lichtenberg. *Principles of Plasma Discharges and Materials Processing*. New York: Wiley, 1994.

[21] Pedroni, E. "Proton Beam Delivery Technique and Commissioning Issues: Scanned Protons." PTCOG Educational Meeting. FL, Jacksonville. 19 May 2008.

[22] Pedroni, Eros. "Status of Hadrontherapy Facilities Worldwide." EPAC. Genoa. 24 June 2008.

[23] Reiser, M. *Theory and Design of Charged Particle Beams*. New York: Wiley, 1994.

[24] Ripert, M., A. Buechel, A. Peters, J. Schreiner, and T. Winkelmann. "A LOW ENERGY ION BEAM PEPPER POT EMITTANCE DEVICE." *HIT, Heidelberg Germany*

[25] Schmelzbach, P. A., A. Barchetti, H. Einenkel, and D. Goetz. "A Compact, Permanent Magnet, ECR Ion Source for the PSI Proton Accelerator." *Cyclotrons and Their Applications, International Conference* (2007): 292-94.

[26] Stockli, Martin P. "Measuring and Analyzing the Transverse Emittance of Charged Particle Beams." *Beam Instrumentation Workshop 2006: Twelfth Beam Instrumentation Workshop, Batavia, Illinois, 1-4 May 2006 : BIW06*. By Thomas S. Meyer and Robert C. Webber. Melville, NY: American Institute of Physics, 2006. 25-62.

[27] Unkelbach, Jan, and David Craft. "Dose Calculation and Interactions of Protons with Tissue." Physics of Proton Therapy. United States, Cambridge. 2011.

[28] Wangler, T., F. Merrill, L. Rybarcyk, and R. Ryne. "Space Charge in Proton Linacs." *Workshop on Space Charge Physics in High Intensity Hadron Rings* (1998)

[29] Xie, Zu Q. *The Effect of Space Charge Force on Beams Extracted from ECR Ion Sources.* Thesis. Michigan State University, 1989.